University of Windsor

Scholarship at UWindsor

1-1-2005

Water and thermal management in a single PEM fuel cell.

Yi Zong
University of Windsor

Follow this and additional works at: https://scholar.uwindsor.ca/etd

Recommended Citation

Zong, Yi, "Water and thermal management in a single PEM fuel cell." (2005). *Electronic Theses and Dissertations*. 6938.
https://scholar.uwindsor.ca/etd/6938

NOTE TO USERS

This reproduction is the best copy available.

UMI®

WATER AND THERMAL MANAGEMENT IN A SINGLE

PEM FUEL CELL

By

Yi Zong

A Thesis
Submitted to the Faculty of Graduate Studies and Research
through the Department of Mechanical, Automotive & Materials Engineering
in Partial Fulfillment of the Requirements for
the Degree of Master of Applied Science at the
University of Windsor

Windsor, Ontario, Canada

2005

(c) 2005 Yi Zong

Canada

ABSTRACT

The fuel cell is an electrochemical device that employs electrochemical reaction to produce electricity and thermal energy with water as the by-product. Because of its zero-emission nature, it plays a more and more important role in future energy conversion system. Among the various types of fuel cells, the proton-exchange membrane fuel cell (PEMFC) has been considered as a promising choice for the automobile since it operates at near-room temperature.

In this thesis, a two-dimensional water and heat management model has been developed to simulate the energy, fluid and mass transfer processes inside a PEM fuel cell unit. Since there is water transport across the membrane, the energy balance equation involves the following items: the electro-chemical reaction released energy, output electrical energy, sensible heat carried by flow, latent heat associated with water evaporation and condensation in the flow channel, cooling heat and the heat loss to environment. Based on this model, the fluid parameters can be predicted along the channels of both cathode and anode sides, such as: pressure drop, air temperature, hydrogen temperature, stack temperature, relative humidity, water vapor mole fraction, water liquid fraction, density, viscosity, Reynolds number, velocity volume flowrate, required pumping power, current density, output voltage and so on.

The simulation results in this research are verified very well by experiments under the similar working conditions. It shows that this model can effectively describe the flow behavior inside the PEM fuel cell. It has the potential to be a useful

iii

engineering tool for PEM fuel analysis and design. In addition, the simulations indicate that factors like the relative humidity, the liquid water and temperature distribution play important roles in attaining high performance.

iv

To my parents, sister and brother

ACKNOWLEDGEMENTS

I would express my sincere appreciation to my advisor Dr. Biao Zhou for his support, encouragement and guidance throughout my Master program. I am so indebted to him for inspiring me to pursue a career in the Fuel Cell.

Also, I would like to thank Dr. Gary Rankin, Dr. Huapeng Wu, Dr. William Altenhof who gave useful advice on my thesis. I was both challenged and motivated by their encouragement and high academic standard. Special thanks also go to Dr. Andrzej Sobiesiak for providing the invaluable support in our experiments.

I would like to thank my colleagues and friends: Xiaochen Yu, Wenbo Huang and Peng Quan, Weixiang Yang, and Chunyi Xia for providing so many helpful suggestions, enduring support and cooperation, which make this work much easier. In addition, I thank all my friends in University of Windsor for their kindness, patient, generosity and humor, which bring so much joy and meaning to my life.

I would like to thank Zhengrong Yao for his invaluable help in the academic writing. I am very grateful to my friends: Wei Shen, Bin Song, Feng Li and for all the happiness they brought into my life.

Finally, I would like to thank my parents for their selfless and endless love.

vi

TABLE OF CONTENTS

LIST OF FIGURES

ix

x

xi

NOMENCLATURE

a	water vapor activity in stream
A_c	the heat transfer area between stack and flow in a control volume (cm^2)
A_{cross}	the cross-section area of channel (cm^2)
A_s	the cross-section area of stack (cm^2)
A_{cool}	the heat transfer area between stack and coolant (cm^2)
C_{pi}	heat capacity of species i $(J\ mol^{-1}\ K^{-1})$
C_{MW}	concentration of water at interface of the membrane $(mol\ cm^{-3})$
d	channel height (cm)
D	hydraulic diameter of channel (cm)
D°	a parameter used in the expression for diffusion coefficient of water $(cm^2\ s^{-1})$
D_w	diffusion coefficient of water $(cm^2\ s^{-1})$
f(x)	friction factor
F	Faraday constant, 96487 C/equivalent
h	channel width (cm)
I	current (A)
I(x)	current density $(A\ cm^{-2})$
I°	exchange current density for the oxygen reaction $(A\ cm^{-2})$

k	thermal conductivity of the stream ($W\,m^{-1}\,°C^{-1}$)
k_c	evaporation and condensation rate constant (s^{-1})
L	length of channel (cm)
M_i	molecular weight of species i ($g\,mol^{-1}$)
M	equivalent weight of a dry membrane ($g\,mol^{-1}$)
N	mole number of species in the stream ($mol\,s^{-1}$)
n_d	electro-osmotic drag coefficient (number of water molecules carried by per proton)
NE	number of electrons ($A^{-1}s^{-1}$)
N_{ch}	number of channel (s)
P	cell total pressure (Pa)
p_i	partial pressure of species i (Pa)
dp	pressure drop (Pa)
P_{pump}	pumping power (W)
q	energy ($J\,s^{-1}$)
Q	volume flowrate ($m^3\,s^{-1}$)
Re	Reynolds number
R_u	the ideal gas constant ($8.3144\,J\,mol^{-1}\,K^{-1}$)
RH	relative humidity
S	entropy ($J\,mol^{-1}\,K^{-1}$)
t	thickness (cm)

T	temperature of stream (K)
T_s	temperature of stack (K)
U	overall heat-transfer coefficient (J s^{-1} cm^{-2} °C^{-1})
V	flow velocity (m s^{-1})
V_{cell}	cell voltage (V)
x	direction along the channel length
y	direction normal to the channel length

Greek

α	excess coefficients of air (oxygen)
α_{area}	reaction area coefficient
β_{O2}	mole fraction of oxygen in air (20.9%)
β_{H2}	mole fraction of hydrogen (100%)
μ	dynamic viscosity (N s m^{-2})
ρ	density (kg m^{-3})
η	overpotential for the oxygen reaction (V)
ϕ	water content in stream
$\rho_{m,dry}$	density of a dry membrane (g cm^{-3})
σ_m	membrane conductivity (Ω^{-1} cm^{-1})

Subscripts

0	in the standard state
1A	per ampere
air	dry air
avg	average
A	anode
C	cathode
cell	the unit fuel cell
concentration	the concentration of species in the streams
cool	cooling system
drag	electro-osmotic drag
e	electron
ele	electricity
gas	species except water vapor and water liquid
gen	generated
H_2	hydrogen
H_2O	produced water
heat	heat
in	inlet of channel
latent	latent heat
loss	energy released to environment
m	membrane

MW	water in membrane
N_2	nitrogen
O_2	oxygen
oc	open circuit
pressure	the partial pressure in the streams
pump	the pump supplied the reactants to fuel cell
rxn	reaction
room	environment
sat	saturation
sen	sensible
stack	the stack of fuel cell
systema	closed system
vapor	water vapor in the flow
liquid	liquid water in the flow
water	all water including vapor and liquid in the flow
#	cathode or anode

1. INTRODUCTION

Most current automobiles are driven by internal combustion engines which consume fossil fuel and generate air pollution. With the increasing public concerns of environmental protection, it is predictable that more and more strict regulations will be enforced to reduce or limit the emission of these vehicles in the future. For example, California's zero emission vehicle (ZEV) mandate [1] requires 10% of the vehicles sold by the automotive manufacturers after year 2004 to be ZEVs [2]. Similarly, European auto companies are required to meet their voluntary carbon dioxide emission limits set by the European Union [3]. According to the Kyoto Protocol, the international community is committed to cut greenhouse gases emission step by step. The Carbon Dioxide (CO_2) emitted by automobiles is one of the most important parts of greenhouse gases. Governments like Canada have already invested a lot in exploring new ways to replace the internal combustion engine in automobiles. Among all the technical proposals, fuel cell is one of the most potential and feasible solutions to achieve this goal. The benefits of using fuel cells are as follows [4]: firstly, fuel cells consume hydrogen instead of the exhaustible fossil fuel, which eventually protect our natural resource and environment; secondly, fuel cells emit only water, therefore, there is no pollution at all. Among all the currently existing fuel cells, the proton exchange membrane (PEM) fuel cell has been widely considered as one of the most promising candidates for automobiles since it has one additional advantage over many other fuel cells: the PEM can operate at room temperature for

1

quick startup. In this thesis, the research will focus on the PEM fuel cell related topics.

Before continuing the discussion of this research topic, it is necessary to review a little about the progress of fuel cell research and development. The fuel cell idea has been known for over 150 years. Although the first fuel cell was built by Sir William Grove in 1839, it was until the 1960's that the PEM fuel cell was invented at General Electric in the U.S. This PEM fuel cell was used by NASA on their first manned space vehicle. Since the early 1980s, the British Royal Navy began to adopt this technology in their submarines. Since then, many companies and institutes around the world actively work on fuel cells to improve its safety, performance and lower its costs. In 1995, a Vancouver company named Ballard Power, tested the PEM cell on the buses of Vancouver and Chicago, and later DaimlerChrysler put the PEM fuel cells in their experimental vehicles as well.

Although the PEM fuel cell technology has been successfully demonstrated, the performance of the fuel cells still needs to be improved before they can be used as viable commercial products. One of the technical issues in fuel cell development is water and thermal management. On the one hand, fuel cells, just like any other energy conversion device, are not 100% efficient [5]. Part of fuel energy cannot be converted to useful electrical energy and has to be rejected as waste heat to ambient by convection. Hence, heat rejection becomes an important consideration in fuel cell design. Furthermore, PEM fuel cells need water to humidify the air and fuel. They also produce water during the reactions. It is necessary to remove the excess water

2

and achieve "water balance" inside the PEM fuel cell. Since previous research showed that water and heat management have a great influence on the fuel cell's performance, a further study about the flow behavior inside the PEM module can be very meaningful.

The aim of this work was to develop a steady-state, two-dimensional mathematical model with mass and heat transfer, water balance in a single PEM fuel cell operated under the low temperature and low pressure to provide an understanding of the flow characteristics in the channels of fuel cells and enable the designers to optimize their designs by a numerical trial-and-error method. The trends of pressure drop, temperature, relative humidity of reaction flow, water vapor mole fraction, water liquid fraction and stack temperature along the channels are predicted in this work.

3

2. PRINCIPLES OF PEM FUEL CELL

This chapter describes the components of the fuel cell system first. Then, the principle of a single PEM fuel cell will be reviewed. After that, the detail concerning the issue of water and heat management inside the PEM fuel cell will be discussed. If you are familiar with the fundamentals related to these fields, you can skip this chapter.

1. Fuel Cell System

A simple PEM fuel cell system will include at least the following basic components in the design: the fuel cell stack which consists of a number of single fuel cells, the fuel supply system, the air supply system, the cooling and humidification system. The fuel cell stack is a key component inside which the electrochemical reactions occur. It generates the electricity and provides power to an external circuit. Since there will be thermal energy produced as the byproduct, a cooling system is needed to remove the waste heat. The fuel supply system, possibly a hydrogen storage tank or a hydrogen-produced reformer, will provide hydrogen to the anode side of fuel cell stack. The air supply system, which may be composed of additional equipment like a pump or blower, will provide cleaned and conditioned ambient air to the cathode side of fuel cell stack. Generally, the fuel cell unit will operate at 70~90°C for optimal performance. The reaction of fuel cell will also produce water which can be

4

directly emitted to the ambient. To improve the efficiencies of the fuel cell unit, both

the hydrogen and air supply need to be humidified before they enter the fuel cell

stack. Part of water produced by the fuel cell can be reused to fulfill this purpose. The

details regarding the reactions inside the fuel cell will be further explained in the next

section.

2. Single PEM Fuel Cell

A typical sandwich construction of a single PEM fuel cell is shown in Fig. 1.

It consists of a proton-exchange membrane, two active layers and electrodes, and two

plates with channels at cathode and anode.

The proton-exchange membrane is a very thin polymer membrane which lies

in the middle of a single cell and between the two active layers and electrodes. The

most well-known polymer material is called Nafion made from fluoroethylene and

manufactured by Dupont. Other kinds of membranes are also available, such as those

made from new perflourosulfonic acids. Many fuel cell companies claim that they

developed their own membrane which is more efficient and durable. Commonly, the

thickness of membrane is between 0.0508 mm to 0.1778 mm [4]. Thin membranes

generally have better performance, lower mechanical stability and lower overall life

times.

The proton-exchange membrane plays an important role in a PEM fuel cell

since it has a set of very special characteristics. One of its characteristics is that only

5

hydrogen ions and water molecules can migrate through the proton-exchange membrane. The hydrogen gas, oxygen gas and electrons, on the other hand, cannot pass through it. Therefore, even thought the proton-exchange membrane separates reactants, it will allow the electrochemical reaction to happen. Another property of the proton-exchange membrane is that the proton conductivity is directly proportional to the water content. The higher the water content is, the more the water molecules can pass through the membrane and a better performance can be obtained. However, sometimes there is too much water to be fully taken away by the reactant. The water will block the pores in the electrodes and slow down the reaction speed, which leads to the downgrade of the fuel cell performance. Therefore, the water management in the proton-exchange fuel cell is considered to be a significant factor which affects the fuel cell performance.

The active layer and electrode is a thin layer of porous carbon cloth or cloth paper that contains a light platinum coating on one face of each electrode. In the early days of PEM fuel cell development, platinum coating was used at the rate of 28 mg cm^{-2}. This is a major factor in the cost of a PEM fuel cell. Recently, the usage of platinum has been reduced to around 0.2 mg cm^{-2} [6], which cuts the price of PEM fuel cell greatly. Usually, a fuel active layer and electrodes, a membrane and an oxidant active layer and electrodes are assembled as a very thin item, which is called the membrane electrode assembly (MEA).

The outer parts of a single PEM are plates which are usually made from stainless steel or carbon graphite, containing many tiny channels. Those plates have

6

the following functions: 1. deliver hydrogen and oxygen to the MEA; 2. remove the water and waste heat that are generated in the fuel cell reaction; 3. collect the current produced by MEA. The reactants (hydrogen and oxygen) flow along the channels at the anode plates and cathode plates respectively. When the hydrogen gas flows along the channels, it diffuses into the active layer and contacts the platinum catalysts which is build in active layer. Meanwhile, the hydrogen releases electrons and creates hydrogen ions. The electrochemical reaction on the anode side is [4]: $2H_2 \rightarrow 4H^+ + 4e^-$. On the cathode side active layer, an electrochemical reaction takes place when oxygen combines with hydrogen ions, which migrated through the membrane, and the electrons. Water is produced and heat is released. The chemical reaction that occurs on the cathode side is: $O_2 + 4e^- + 4H^+ \rightarrow 2H_2O + q_{rxn}$.

3. Water and Thermal Management

Before the PEM fuel cell becomes a commercial solution for automotive applications, there are several important technical issues that need to be resolved. One of these issues is the water and thermal management in the fuel cell. Proper water and thermal management is essential for achieving the optimal performance for the PEM fuel cell [7, 8]. Some reasons for studying the topic of the water and thermal management in the fuel cell are listed as follows:

1. Water starvation in membrane. As mentioned in section 2.2, the membrane in the fuel cell needs to be hydrated during its operation. According to Prater [9],

7

if the membrane is not humidified enough, high ionic resistance will exist. In the worst situation, this may lead to the failure of the reaction. Maintaining an optimal working condition, such as pressure and humidity, on both the cathode and anode side is important in achieving high efficiency in the fuel cell.

2. Water flood in cathode. The electrochemical reaction will produce water as the byproduct. A part of the water can be recovered to hydrate the PEM membrane. The rest of water will remain in the channels. If the water in the channels can't be discharged in time, it will block the pores of the electrode and slow down the electrochemical reaction. By achieving better water balance inside the fuel cell, we may improve the fuel cell performance. To successfully adjust the water balance, it is necessary to investigate the flow behavior inside the fuel cell unit.

3. Waste heat removal. The PEM fuel cell, like any other energy-producing device, cannot achieve a 100% efficiency. Heat is also emitted during the chemical reaction that generates the electricity. The heat will affect the temperature, pressure and many other parameters of the steam in both the anode and cathode channels. To keep the fuel cell operating under the optimal working condition, any additional heat should be removed from the system.

It is evident that the water and thermal management issues have direct influence on the performance of fuel cell. Many studies have attempted to understand the physical process occurring inside the fuel cell and built better models to describe

8

them. In this research, interest is on the investigation of fluid and thermal fields inside a single PEM fuel cell which operate at near room temperature and atmosphere pressure. The following sections of this thesis are organized as follows: Chapter 3 will provide a literature review, which will present the current progress in the related research fields in detail. The physical model of PEM fuel cell is described in Chapter 4. Chapter 5 and Chapter 6 discuss the simulation process, result and analysis, respectively. Finally, the conclusions are addressed in Chapter 7.

9

3. LITERATURE REVIEW

Costamagna *et al.* [10] gave a very good review about the fuel cell science and technology up to the year 2000. Another recent review made by Yao *et al.* [11] presents both empirical performance models and theoretical models. I n the early 1990's, the pioneering work was done. Bernardi [12] presented a water balance calculation and the sensitivity of water balance to input conditions. However, this study did not involve a detailed membrane model. Bernardi *et al.* [13] and [14] formulated one-dimensional and isothermal models for the partial system of the gas-diffusion cathode, active catalyst layer, and ion-exchange membrane. Only the direction perpendicular to the membrane is considered. Springer et al. [15] presented a one-dimensional PEM fuel cell model. The model employs a water diffusion coefficient, electro-osmotic drag coefficients, and membrane conductivities to predict the change of membrane resistance with current density. Also, the results of their model are partially validated with experimental data. However, the temperature is assumed to be a constant and the model is unable to simulate the real flow behavior along the channels of the PEM fuel cell. Later on, Springer *et al.* [16], [17] developed another detailed model of the transport phenomena in the catalyst layers. The model in Springer *et al.*[17], however, did not consider the water transport in the fuel cell.

Compared with a one-dimensional model, the two-dimensional mathematical model is preferable for water and heat management prediction, such as, the temperature, pressure and water changes along the channel. Fuller *et al.* [18]

10

developed a non-isothermal model by including the material balances in the channel, the concentration and temperature gradients along the channel as well as across the membrane surface. Nguyen *et al.* [19] studied the variation in current density, water transport, and flow temperatures along the channel. They also model the effect of varying anode inlet humidity. Subsequently, an advanced model was developed by Yi *et al.* [20] to compare different fuel cell designs with coflow and counterflow heat exchangers. In this analysis, they include the thermal mass of the stack, account for the impact of the pressures difference between anode and cathode on water transport in the cell. However, there is no clear validation of results in both of the analyses. Mosdale *et al.* [21] give a review of the work that has been done at Texas A&M University. In this review, the various models are compared and the effect of different humidification on the performance of the fuel cell is discussed. Unfortunately, this paper does not give the exact details of their modeling approaches. Amphlett et al. [22], [23] of the Royal Military College of Canada have developed PEM fuel cell models that are based on both the theoretical mechanistic analysis and empirical data. They perform an empirical treatment of the membrane and explain the water transport processes in the membrane. Nevertheless, this model cannot predict some parameters, such as anode humidification, temperature, pressure and so on. Researchers like Marr *et al.* [24], Dannenberg *et al.* [25], Hertwig *et al.* [26], Ge *et al.* [27] and Xue *et al.* [28] have been doing fuel cell modeling for many years and have made very impressive progress. Those models emphasized important characteristics of the membrane, electrodes, as well as a detail description of the water content in the

membrane. In order to simplify the process, some models assume that there is no temperature drop and pressure drop along the channel. Most models are assumed to be operated at high temperature (e.g. 90°C - 100°C), high pressure (e.g. 3 atm), and the constant temperature of solid phase. However, the general PEM fuel cell applied in the automobile is operated at low temperature (e.g. 23°C - 40°C) and low pressure (e.g. 1.3 atm for 1kw portable applications). In addition, the pressure drop along channel is quite obviously in most PEM fuel cells. This parameter is very critical in designing the PEM fuel cell. It can be used to not only choose suitable pumps to supply reactants to fuel cell, but also discharge water produced by electrochemical reaction. However, few previous papers address this problem in detail.

In order to face these challenges, in the present study, a steady-state, two-dimensional model with pressure effects, water phase-change effects and detailed mass and heat transfer in a unit fuel cell was developed. The trends of pressure drop, flow temperature, relative humidity of reaction flow, water vapor mole fraction, water liquid fraction, and stack temperature along the channels are predicted. The effect of inlet water content and temperatures of the reactants on the performance of a PEM fuel cell is investigated in detail.

4. MATHEMATICAL MODEL

Fig. 1 shows that the typical construction of a PEM fuel cell. In the present study, two coordinate axes are chosen. The x-axis is parallel to the gas channels. The temperature, pressure and concentration of gas flow will be calculated along this direction. The y-axis is perpendicular to the membrane. The hydrogen ions and water molecules transport from anode to cathode along this direction. The model includes the following parts:

- Mass balance

- Energy balance

- Pressure drop

- Cell output voltage

4.1 Basic Assumptions

In the present model, the water transport mechanisms in the membrane are based on the study by Yi *et al.* [19]'s study. Some corresponding assumptions are listed as follows.

1. Only water vapor can diffuse into the electrode and pass through the membrane.

2. The electrode layer is "ultra thin", gas diffusion through the electrode porous layer is neglected.

13

3. The gases and water vapor are fully mixed, and the mixture is ideal gas.

4. Liquid water exists only in the form of small droplets and the volume is negligible.

5. Water vapor is produced in the electrochemical reaction.

6. No voltage drop exists along the flow channels.

7. The channels in each unit cell have the same geometry and same surface roughness;

8. Single channel is assumed to represent the unit cell for numerical simulations;

9. The temperature of the solid (including MEA and plates) is assumed to be uniform in the y-direction.

4.2 Mass Balance

Fig. 2 shows the mass balance in a unit fuel cell. The amount of inlet gases is calculated according to the amount of gases consumed by the electro-chemical reaction for PEM fuel cell $2H_2 + O_2 = 2H_2O + 4e^-$. One equivalence of electrons is 1 mole of electrons or 6.022×10^{23} electrons (Avagadro's number). This quantity of electrons has the charge of 96487 coulombs (C) (Faraday's Constant). Therefore, the charge of a single electron is 1.602×10^{-19} C. One ampere of current is defined as 1C/Sec. As a result, the mole number of electrons for one ampere of current is as follows:

14

$$n_e = \frac{NE_{1A}}{6.022 \times 10^{23}} = 1.03656546 \times 10^{-5} \; mole/(A \cdot s) \qquad (1)$$

where NE_{1A} represents the number of electrons in one ampere. It can be calculated by $NE_{1A} = 1/1.602 \times 10^{-19}$. Based on the reaction equation, the theoretical mole numbers of consumed oxygen and hydrogen, and produced water for one ampere current output can be obtained by the following equations:

$$n_{O_2,1A} = \frac{1}{4} n_e \qquad (2)$$

$$n_{H_2O,1A} = \frac{2}{4} n_e = \frac{1}{2} n_e \qquad (3)$$

$$n_{H_2,1A} = \frac{2}{4} n_e = \frac{1}{2} n_e \qquad (4)$$

The excess coefficients for air (oxygen) or hydrogen is defined as:

$$\alpha = \frac{\text{actually supplied mole number of air (oxygen) or hydrogen}}{\text{theoretically consumed mole number of air (oxygen) or hydrogen}} \qquad (5)$$

Therefore, the supplied oxygen, nitrogen and hydrogen mole numbers can be calculated by the following equations:

$$n_{O_2,in,1A} = \alpha_{O_2} n_{O_2,1A} \qquad (6)$$

$$n_{N_2,in,1A} = n_{O_2,in,1A} \times (1 - \beta_{O_2}) / \beta_{O_2} \qquad (7)$$

$$n_{H_2,in,1A} = \alpha_{H_2} n_{H_2,1A} / \beta_{H_2} \qquad (8)$$

15

where β_{O2} is the mole fraction of oxygen in air ($\beta_{O2} = 20.9\%$) and β_{H2} is that of the

hydrogen in anode ($\beta_{H2} = 1$ in the present study).

For generating I amperes of current, the molar flowrates of oxygen, nitrogen

and hydrogen for the single channel are evaluated in (mol/s) as:

$$N_{C,O_2,in} = I \times n_{O_2,in,1A} / N_{ch} \tag{9}$$

$$N_{C,N2,in} = N_{C,O2,in} \times \frac{(1 - \beta_{O_2})}{\beta_{O_2}} \tag{10}$$

$$N_{A,H_2,in} = I \times n_{H_2,in,1A} / N_{ch} \tag{11}$$

The components of the mixture vary along the channels and the local molar

flowrates in channel are defined as follows:

$$\frac{dN_{C,O_2}(x)}{dx} = -n_{O_2,1A} \times I(x) \times h \times \alpha_{area} \tag{12}$$

$$\frac{dN_{C,N_2}(x)}{dx} = 0 \tag{13}$$

$$\frac{dN_{A,H_2}(x)}{dx} = -n_{H_2,1A} \times I(x) \times h \times \alpha_{area} \tag{14}$$

where $\square_{area}$ is the reaction area coefficient that accounts for the land area for reaction

due to gas diffusion from the channel to diffusion layer.

The variations of vapor and liquid water along the channels are more

complicated. Vapor water transport and condensation, and liquid water evaporation

are considered in this model. There are three water transport mechanisms across the

16

membrane, according Yi *et al.* [19]: (a) electro-osmotic drag - since the hydrogen ions pass through the membrane, the water molecules are carried from the anode to the cathode; (b) back-diffusion by the concentration gradient of water - because the water concentration is different, some water molecules diffuse from the cathode to the anode; (c) convection by the pressure gradient - water moves from higher-pressure side to the lower one. In a calculated volume, there is no potential gradient in the x-direction. The electro-osmotic drag flux (mol/s) in the y-direction is as follows [18]:

$$N_{drag}(y) = \frac{n_d(x)I(x)}{F} \tag{15}$$

where $I(x)$ is the local current density of the fuel cell, F is Faraday's constant. n_d is the electro-osmotic drag coefficient which represents the number of water molecules carried by one proton. It is calculated by [18]:

$$n_d(x) = \begin{cases} 0.0049 + 2.02a(x) - 4.53a^2(x) + 4.09a^3(x) & (\ 0 < a(x) \le 1) \\ 1.5849 + 0.159(a(x) - 1) & (\ a(x) > 1) \end{cases} \tag{16}$$

where $a(x)$ is the activity of water vapor in membrane. Since the membrane is placed between the cathode and anode, the water vapor activity in the membrane is affected by the water vapor activity at both cathode and anode. A weighted average water activity for the water vapor activity in the membrane is employed. The water vapor activity at anode or cathode $a_\#(x)$ is defined as [18]:

17

$$a_{\#}(x) = \frac{N_{\#,vapor}(x)}{\sum_i N_{\#,i}(x)} \times \frac{p_{\#}(x)}{p_{\#,sat}(x)} \qquad (\textit{i, the species in the flow stream \#}) \qquad (17)$$

The water vapor activity at the membrane is defined as:

$$a_M(x) = \alpha_M a_A(x) + (1 - \alpha_M)a_C(x) \qquad (18)$$

where α_M is the weight coefficient. Thus, the water vapor activity at the membrane depends on the water activity at both cathode and anode.

The diffusion flux caused by the concentration gradient of water can be written as follows

$$N_{concentration}(y) = D_{MW}\left(\frac{\partial c_{MW}}{\partial y}\right) \qquad (19)$$

where the diffusion coefficient of water is as follows [19]:

$$D_{MW} = \begin{cases} (0.0049 + 2.02a(x) - 4.53a^2(x) + 4.09a^3(x))D^{\circ}\exp[2416(\frac{1}{303} - \frac{1}{T_s(x)})] & (\textit{for } 0 < a(x) \le 1) \\ [1.59 + 0.159[(a(x) - 1)]D^{\circ}\exp[2416(\frac{1}{303} - \frac{1}{T_s(x)})] & (\textit{for } a(x) > 1) \end{cases}$$

$$(20)$$

Convection flux caused by pressure gradient [19] is,

$$N_{pressure}(y) = [\frac{c_{MW,C}(x) + c_{MW,A}(x)}{2}] \times \frac{k_P}{\mu_W(x)} \times (\frac{\partial p_{\#,vapor}}{\partial y}) \qquad (21)$$

where $p_{\#,vapor}$ is the water vapor pressure in the anode and cathode channels, respectively. k_p is the permeability of water in the membrane, and $\mu_W(x)$ is the water viscosity. $c_{MW,C}(x)$ and $c_{MW,A}(x)$ are the concentrations of water in cathode and anode respectively, and the expression is given below [18],

$$c_{MW,\#}(x) = \begin{cases} \dfrac{\rho_{m,dry}}{M_{m,dry}}[0.043 + 17.8a_\#(x) - 39.8a_\#^2(x) + 36.0a_\#^3(x)] & (\textit{for } 0 < a_\#(x) \le 1) \\ \dfrac{\rho_{m,dry}}{M_{m,dry}}[14 + 1.4(a_\#(x) - 1)] & (\textit{for } a_\#(x) > 1) \end{cases}$$

$$(22)$$

where $\square_{m,dry}$ and $M_{m,dry}$ are the density and the equivalent weight of a dry proton exchange membrane. Therefore, the change of water flux along the channel at the cathode can be expressed by

$$\frac{dN_{C,water}(x)}{dx} = [n_{H_2O} \times I(x) + N_{drag}(y) - N_{concentration}(y) - N_{pressure}(y)] \times h\alpha_{area} \qquad (23)$$

The variable trend of water flux in anode can be expressed by

$$\frac{dN_{A,water}(x)}{dx} = [- N_{drag}(y) + N_{concentration}(y) + N_{pressure}(y)] \times h\alpha_{area} \qquad (24)$$

19

The mole number of water condensation or evaporation can be calculated as [18]

$$\frac{dN_{\#,liquid}(x)}{dx} = (\frac{k_c hd}{R_u T_{\#}(x)})[\frac{N_{\#,vapor}(x)}{\sum_i N_{\#,i}(x)} \times p_{\#}(x) - p_{\#,sat}(x)]$$

$$(i,\ the\ gaseous\ species\ in\ stream\ \#) \qquad (25)$$

In order to present the state of vapor water and liquid water, relative humidity (RH) and relative water content (ϕ) are defined as follows:

$$RH_{\#}(x) = \frac{partial\ pressure\ of\ vapor\ water}{saturation\ pressure} \quad or \quad RH_{\#}(x) = \frac{N_{\#,vapor}(x)}{\sum_i N_{\#,i}(x)} \times \frac{p_{\#}(x)}{p_{\#,sat}(x)} \qquad (26)$$

$$and \quad \phi_{\#}(x) = \frac{mole\ number\ of\ water\ (vapor + liquid)}{mole\ number\ of\ water\ in\ saturation} \quad or$$

$$\phi_{\#}(x) = \frac{N_{\#,water}(x)}{\sum_i N_{\#,i}(x)} \times \frac{p_{\#}(x)}{p_{\#,sat}(x)} \qquad (i,\ the\ gaseous\ species\ in\ stream\ \#) \qquad (27)$$

4.3 Energy Balance

As shown in Fig.3, the energy in a unit fuel cell consists of the energy released from chemical reaction, which is the source of energy in fuel cell; the electrical energy for generating power; the heat for increasing the solid phase temperature; the sensible heat for increasing the temperature of flow; the latent heat for water phase changes; the waste heat taken away by coolant; and the heat loss to

20

the environment at the inlet and exit of channel.

The total energy balance is

$$q_{rxn}(x) = q_{elec}(x) + q_{heat}(x)$$
$$= q_{elec}(x) + q(x)_{stack} + \sum q_{\#,sen}(x) + \sum q_{\#,latent}(x) + q_{cool}(x) \tag{28}$$

The energy released from electrochemical reaction is difficult to calculate. In general, enthalpy or entropy is employed to evaluate the energy and electrical work in an electrochemical system. For a reversible cell:

$$q_{heat}(x) = T_0 \Delta S(x) \tag{29}$$

In this study, the entropy is used to calculate the released energy. For the reacting and non-reacting system, the entropy balance for undergoing any process can be expressed as:

$$(S_{in} - S_{out}) + S_{gen} = \Delta S_{system} \tag{30}$$

This means that the change of entropy in a system can be determined by the net entropy transfer and the entropy generated in the system. The difference of the entropy change between a system with chemical reaction and a non-reacting system is that: the entropy relations for the reactants and the products involve the entropies of

21

the components, not entropy changes, which was the case for non-reacting system [29]. Thus, a common base for the entropy of all substances is established by the third law of thermodynamics. Based on the third law of thermodynamics, the entropy has a common universal scale for each chemical compound. The common scale, called the absolute entropy, is based on the fact that the entropy for any pure element is zero at the temperature of absolute zero. For the electrochemical reaction in a PEM system, it is difficult to calculate the reaction heat for the total reaction. However, if one could tell the heat generation in which electrode heat is generated and in which it is absorbed, the corresponding total reaction heat can be calculated easily. For the electrode reaction at the anode, the entropy change can be calculated by:

$$\Delta S_A^0 = 4S_{H^+}^0 + 4S_{e^-}^0 - 2S_{H_2}^0 \tag{31}$$

where S^0 is the absolute values of species at the standard state: $T_0 = 298.15$ K, $P_0 = 1$ bar. The numerical values for the species are taken from [20] and [21]. The entropy change at anode is: $S_A = 0.208$ J/(mol K) [30]. In the same way, the entropy change for the cathode reaction, can be calculated by:

$$\Delta S_C^0 = 2S_{H_2O}^0 - S_{O_2}^0 - 4S_{e^-}^0 - 4S_{H^+}^0 \tag{32}$$

The entropy change at the cathode is: $S_C = -326.36$ J/ (mol K) [30]. The absolute entropy of the species i at the temperature T and pressure P can be calculated from

22

$$S_i(T, P, x) = S_i^0 + \int_{T_0}^{T} \frac{Cp_i(x)}{T} dT + \int_{P_0}^{P} [-\frac{\partial v_i(x)}{\partial T(x)}] dp \qquad (33)$$

where $v_i(x)$ is the specific volume of flow at the location of x. Considering the total

reaction in a cell, the reaction heat flux (J/s) can be calculated for the reversible

process as:

$$q_{heat}(x) = [\frac{\Delta S_A(x)}{2F} + \frac{\Delta S_C(x)}{4F}] T_s(x) \times I(x) \times h \times \alpha_{area} \times dx \qquad (34)$$

For the real irreversible process, due to the ohmic loss and reaction

resistance, some of the electrical energy is turn into the released heat. The total

reaction heat flux can be expressed:

$$q_{heat}(x) = [\frac{\Delta S_A(x)}{2F} + \frac{\Delta S_C(x)}{4F}] T_s \times I(x) \times h \times \alpha_{area} \times dx - \eta(x) \times I(x) \times h \times \alpha_{area} \times dx$$

$$(35)$$

If the numerical value of $q_{heat}(x)$ is negative, it means that the chemical reaction emits

heat to the surrounding.

The electrical energy (J/s) is:

$$q_{elec}(x) = V_{cell}(x) \times I(x) \times h \times \alpha_{area} \times dx \qquad (36)$$

The sensible heat of mixture flow at cathode channel (J/s) is:

$$dq_{\#,sen}(x) = \sum_i [N_{\#,i}(x)Cp_i(x)]dT_\#(x) \quad (i,\text{ the gaseous species in stream \#}) \qquad (37)$$

The latent heat for water vapor condensation or liquid water evaporation at cathode or anode channels (J/s):

$$dq_{\#,latent}(x) = [H_{\#,vapor}(x) - H_{\#,liquid}(x)] \times dN_{\#,liquid}(x) \qquad (38)$$

In this model, the heat taken by the coolant is considered and expressed by:

$$q_{cool}(x) = U_{cool} \times A_{cool}[T_S(x) - T_{cool}] \qquad (39)$$

where U_{cool} is the heat transfer coefficient between stack and coolant, A_{cool} is the area of heat transfer.

When the streams flow along the channels, they will gain or lose heat due to the heat transfer between the fluid and stack. Therefore, the temperature of flow depends on the stack temperature and the latent heat as well, which can be calculated as follows:

24

$$\sum_i [N_{\#,i}(x)C_{p,i}(x)]\frac{dT_\#(x)}{dx} = [H_{W,vapor}(x) - H_{W,liquid}(x)]\frac{dN_{\#,liquid}(x)}{dx} + U_\# h[T_S(x) - T_\#(x)]$$

(40)

$U_\#$ represents the heat transfer coefficient between the flow stream # and stack. The term on left side of the equation represents the heat flux obtained by gaseous flows. The first term on the right side of the equation accounts for the enthalpy change due to condensation or evaporation of water in the channels, which can be calculated using equation (40). The second term on the right side of the equation is for the convection heat flux between the stream and the stack.

$$H_{\#,vapor}(x) - H_{\#,liquid}(x) = 45070 - 41.9[T_\#(x) - 273] + 3.44 \times 10^{-3}[T_\#(x) - 273]^2$$
$$+ 2.54 \times 10^{-6}[T_\#(x) - 273]^3 - 8.98 \times 10^{-10}[T_\#(x) - 273]^4$$

(41)

The stack temperature varies with along the channels. It is determined by the local current density, local latent heat, and local cooling heat. It is calculated by the following energy balance equation:

$$A_s k \frac{d^2T_S(x)}{dx^2} - [N_{C,liquid}(x) + N_{A,liquid}(x)]C_{P,water}\frac{dT_S(x)}{dx}$$
$$= -A_C U_\#[T_A(x) + T_C(x) - 2T_S(x)] - A_{cool} U_{cool}[T_{cool}(x) - T_S(x)]$$
$$- [H_{A,vapor}(x) - H_{A,liquid}(x)]\frac{dN_{A,liquid}(x)}{dx} - [H_{C,vapor}(x) - H_{C,liquid}(x)]\frac{dN_{C,liquid}(x)}{dx}$$
$$+ [(\frac{\Delta S_A(x)}{2F} + \frac{\Delta S_C(x)}{4F})T_S(x) - \eta(x)] \times I(x) \times h \times \alpha_{area}$$

(42)

25

where k is the thermal conductivity of the stack. A_S represents the cross-section area of the stack along the flow direction, A_C represents the heat transfer area between stack and flows, and A_{cool} is the heat transfer area between stack and coolant. The term on the left side of equation represents energy flow by the conduction in the stack of the cell along the gas flow path (x-direction). The temperature distribution normal to gas flow (y-direction) is assumed to be uniform. The first term on the right side of equation is for convective heat transfer between the streams in the channels and the stack of cell. The second term on the right side of equation accounts for convective heat transfer between the stack of cell and coolant. The temperature of coolant is assumed to be constant along the channels. The third and fourth terms represent the energy taken or released from the phase changes of water in the anode or cathode flow (latent heat), which can be calculated in equation (40). The last term represents heat generation by the reversible chemical reaction process.

4.4 Pressure Drop

The pressure drop of the gas mixture in the fuel cell flow channel was rarely considered in currently available fuel cell research publications. But, in industrial design, it is a significant parameter simply because it directly affects the efficiency of system.

The saturation pressure (Pa) can be expressed in terms of the local

26

temperature [31].

$$p_{sat}(x) = 1.013 \times 10^5 \times 10^{-2.1794 + 0.02953\,(T_{\#}(x)-273)-9.1837\times10^{-5}\,(T_{\#}(x)-173)^2 + 1.4454\times10^{-7}\,(T_{\#}(x)-273)^3}$$

(43)

Based on the assumption that the mixture is regarded as an ideal gas, local volumetric flow (m³/s) in the cathode and anode can be calculated using the ideal-gas law.

$$Q_{\#}(x) = \sum_{i} N_{\#,i}(x) \times R_u \times \frac{T_{\#}(x)}{p_{\#}(x)} \qquad (\text{i, the gaseous species in stream \#})$$ (44)

The local velocity (m/s) in the cathode and anode can be calculated as follows,

$$V_{\#}(x) = \frac{Q_{\#}(x)}{A_{\#,cross}}$$

(45)

where $A_{\#,cross}$ is the cross-section area of channel.

Since the mole fraction of gases in the channel varies, local density (kg/m³) also varies with the different components in the flow. It can be calculated from:

$$\rho_{\#}(x) = \sum_{i}[\frac{N_{\#,i}(x)}{\sum_{i} N_{\#,i}(x)} \times \frac{M_{\#,i}}{1000}] \times \frac{p_{\#}(x)}{T_{\#}(x) \times R_u} \qquad (\text{i, the gaseous species in stream \#})$$

27

Local dynamic viscosity can be calculated by interpolation. $\mu_{i,100}$ is the gas dynamic viscosity at 100°C, and $\mu_{i,0}$ is the gas dynamic viscosity at 0°C. The temperature range of flow in the calculated cases is 0 - 100°C, so, the local dynamic viscosity is

$$\mu_{\#}(x) = \sum_{i} \{ \frac{N_{\#,i}(x)}{\sum_{i} N_{\#,i}(x)} \times [\frac{T_{\#}(x) - 273}{100 - 0} \times (\mu_{i,100} - \mu_{i,0}) + \mu_{i,0}]\}$$

(*i, the gaseous species in stream #*)   (47)

For laminar flow, pressure drop in each control volume can be expressed as (Pa):

$$\frac{dp_{\#}(x)}{dx} = \rho_{\#}(x) \times f_{\#}(x) \frac{V_{\#}^{2}(x)}{2D}$$ (48)

where $f_{\#}(x)$ is the friction factor. D is the hydraulic diameter of the channel. In this model, the channels are straight, so that only friction loss is considered. The local pressure (Pa) is calculated by the pressure at inlet subtracting the pressure drop from the inlet to the current control volume.

$$p_{\#}(x) = p_{\#,in} - \int_{0}^{x} [\frac{dp_{\#}(x)}{dx}]dx$$ (49)

28

The total required pumping power (W) is used by designer to choose the pump to maintain the flow. It is given by:

$$P_{\#,pump} = N_{ch} \times \int_0^L \frac{dp_{\#}(x)}{dx} Q_{\#}(x)dx \qquad (50)$$

4.5 Cell Output Voltage

Cell output voltage is a significant parameter that is used to evaluate the performance of a PEM fuel cell. The goal in this section is to model the potential losses in the gas diffusion layers and membrane, so that the output potential can be accurately predicted. The output voltage of the fuel cell is modeled as the reversible cell voltage minus activation losses, concentration over-potential and ohmic resistance of the electrodes, catalyst layer and membrane

The activation losses [6] are caused by the slowness of the reactions taking place on the surface of the electrodes. A proportion of the power generated is lost in driving the chemical reaction that transfers the electrons to or from the electrode. The ohmic resistance [6] is the straightforward resistance to the flow of electrons through the material of the electrodes and the various interconnections, as well as the resistance to the flow of ions through the electrolyte. This voltage drop is essentially proportional to current density. Concentration losses [6] result from the change in concentration of the reactants at the surface of the electrodes as the fuel is used. Because the reduction in concentration is the result of a failure to transport sufficient

29

reactant to the electrode surface, this type of loss is also often called mass transport loss. The cell potential is expressed as [18]:

$$V_{cell} = V_{oc} - \eta(x) - \frac{I(x)t_m}{\sigma_m(x)}$$ (51)

where V_{oc} is the open circuit potential of fuel cell. $\eta(x)$ refers to the cell over potential which combines activation losses and concentration losses together. It is calculated as follows [18],

$$\eta(x) = \frac{R_u T_s(x)}{0.5F} \ln(\frac{I(x)}{I^\circ p_{C,O_2}(x)})$$ (52)

where I° is the exchange current density at one atmosphere of oxygen, and $p_{C,O2}(x)$ is the partial pressure of oxygen at cathode. $\frac{I(x)t_m}{\sigma_m(x)}$ represents the ohmic loss, it depends on the water activity of membrane, stack temperature and the thickness of membrane. $\sigma_m(x)$ is the membrane conductivity and calculated by the following equation [18],

$$\sigma_m(x) = (0.00514 \times \frac{M_{m,dry}}{\rho_{m,dry}} c_{MW}(x) - 0.00326) \exp(1268 \times [\frac{1}{303} - \frac{1}{T_s(x)}])$$

(53)

30

where,

$$c_{MW}(x) = \begin{cases} \dfrac{\rho_{m,dry}}{M_{m,dry}}[0.043 + 17.8a(x) - 39.85a^2(x) + 36.0a^3(x)] & (for\ 0 < a(x) \le 1) \\ \dfrac{\rho_{m,dry}}{M_{m,dry}}[14 + 1.4(a(x) - 1)] & (for\ a(x) > 1) \end{cases}$$

(54)

The current density is distributed unevenly along the channel. However, when a fuel cell is evaluated, the output current is concerned. Therefore, the average current density is calculated using:

$$I_{avg} = \frac{1}{L} \int_0^L I(x)dx$$

(55)

31

5. SOLUTION PROCEDURE

The main focus of this chapter is how to build the simulation process based on the model which has been discussed in previous chapters. This section will firstly review the related computational methods. Then, the discretization method will be discussed shortly. After that, we will continue with the simulation process and discuss the model parameters which are used in the simulation.

5.1 Review of Computational Methods

Based on previous analysis, the model can be summarized into a set of nonlinear differential equations which include 13 governing equations and 13 unknown variables. Generally, the methods to solve nonlinear differential equations can be categorized into two groups: direct methods and indirect or iterative methods.

One good example of direct methods is Runge-Kutta method, which numerically integrates ordinary differential equations by using additional steps at the predicted mid-point of an interval to cancel out lower-order error terms. Therefore, this method is also called as "predictor-corrector algorithms". The benefit of this method is that it is reasonably simple and robust. Runge-Kutta method, which is sometimes combined with an intelligent adaptive step-size routine, is a good candidate for numerical solution of differential equations

The following equations are the formula of fourth-order Runge-Kutta method

32

[32]:

$$x_{n+1} = x_n + h$$

$$y_{n+1} = y_n + \frac{1}{6}(k_1 + 2k_2 + 2k_3 + k_4) + O(h^5)$$

where

$$k_1 = hf(x_n, y_n)$$

$$k_2 = hf(x_n + \frac{1}{2}h, y_n + \frac{1}{2}k_1)$$

$$k_3 = hf(x_n + \frac{1}{2}h, y_n + \frac{1}{2}k_2)$$

$$k_4 = hf(x_n + h, y_n + k_3)$$

At step n, the value of current point x_n, y_n and the interval between the current point

and next point, h, are already known. Function $f(x, y)$ is the slope of solution curve at

a particular point (x, y). According to the Euler method $y = hf(x, y)$, a y-direction jump

value can be derived. At step $n+1$, x_{n+1} can be simply attained by adding the step

interval h. However, the value of y_{n+1} in the y-direction is much more complex to

decide. In the above formula, k_1 means y-direction jump from the current point to the

next Euler-predicted point; k_2 is far more interesting. Here, we also use Euler's method

to predict a mid-point which lies half-way across the predicted interval. The value of

this predicted mid-point in the x direction is $x_n + h/2$, and $y_n + k_1/2$ in the y direction.

Recalling that function f (x, y) means the slope of solution curve,

$hf(x_n + \frac{1}{2}h, y_n + \frac{1}{2}k_1)$ give us the second y-direction jump k_2; Similarly, k_3 is the

third y-direction jump, but instead of using k_1, we use the k_2 to predict the y-value of

the mid-point; k_4 is the jump value which is based on the predicted right end-point of

33

the interval. As before, the y-value of this predicted point is decided by k_3. Once all the four jump values in y-direction have been calculated, a weighted average formula is used to evaluate the y_{n+1}. To analyse the algorithm, if we can generalize the direct methods by using $y_{n+1} = c\, y_n$, where c is a coefficient that depends upon the method used and the equation being evaluated. The primary reason, which makes the fourth order Runge-Kutta method successful, is that the coefficient c that it produces is almost always a very precise approximation to the actual value.

Although the direct methods are quite straightforward, sometimes it is difficult to implement these algorithms efficiently, especially when it involves large vector and parallel architectures. If the system has a large numbers of equations, the memory requirements may grow out of bounds quickly. On the other hand, iterative methods are relatively easy to program for vector and parallel computation and use less computer memory than the direct methods.

Unlike the direct methods which always try to find an exact solution to the equations system, iterative methods attempt to find the solution by repeatedly solving the system equations by using approximations to the vector. Iterations continue until the solution is within a predetermined acceptable bound on the error. For a system of linear equations system, well-known examples of this kind of algorithm include Gauss-Jacobi, Gauss-Seidel and Tri-diagonal matrix methods. For systems of non-linear equations, the Newton-Raphson method is a commonly used algorithm. The disadvantages of iterative methods are: the total number of operations, typically on the order of N per iteration cycle, cannot be predicted in advance; in addition, it is

34

hard to guarantee the convergence unless the system of equations satisfies fairly strict criteria. The main advantage of iterative methods is that only non-zero coefficients of the equations need to be stored in core memory. A brief explanation of each of these methods is listed as the following.

1. Gauss-Jacobi iteration can be expressed as [33]:

$$\bar{x}_{n+1} = D^{-1} \cdot \bar{b} - D^{-1} \cdot (L + U) \cdot \bar{x}_{n}$$

where D is strictly diagonal matrix, $\bar{b}$ and $\bar{x}_{n}$ are known, and $D^{-1} \cdot (L+U)$ just scales each row of the sum $(L+U)$ by the reciprocal of the corresponding element of D. Since the Gauss-Jacobi algorithm uses all values from the previous iteration, it has the disadvantage of slow convergence.

2. Gauss-Seidel iteration can be written as [33]

$$(D + L) \cdot \bar{x}_{n+1} + U \cdot \bar{x}_{n} = \bar{b}$$

where x_{n+1} can be computed quite easily with simple forward substitution because $(D+L)$ is a lower triangular matrix. The practical advantage of this method over the Gauss-Jacobi algorithm is that as soon as an element of the new solution vector at the iteration $n+1$ has been calculated, it can be used successively for the calculation of the remaining elements of x_{n+1}. Compared

35

with the Gauss-Jacobi algorithm, which only uses elements calculated at the iteration n to approximate the solution at iteration $n+1$, the Gauss-Seidel iteration converges twice as fast as Gauss-Jacobi in the average.

3. Tri-Diagonal Matrix Algorithm (TDMA) [34]: Gauss-Jacobi and Gauss-Seidel iterative methods are easy to implement, but they can be very slow to converge especially when the system of equations is large. In many real situations, the system of equations can be simplified and described in form of tri-diagonal matrix, which means there are only nonzero elements on the diagonal, sub-diagonal and super-diagonal of matrix. Neither Gauss-Jacobi method nor Gauss-Seidel methods has any special treatment to make use of this special situations to improve their performance. Therefore, much computational time is wasted on the calculation of a full matrix, most of these calculations result in zero. In 1949, Thomas developed a technique for rapidly solving tri-diagonal system which is now called the Thomas Algorithm or the Tri-Diagonal Matrix Algorithm (TDMA). TDMA can solve these sparsely populated matrices which have the equations in the form of $Ax=b$, where x and b are vectors, and A is a tri-diagonal matrix. Basically, the TDMA follows the rule of the Gaussian elimination. In a full-matrix Gaussian elimination, TDMA eliminates all values below the main diagonal, solves the final equation, and then uses that value in back-substitution to solve the remaining equations. For an n-dimensional matrix A, instead of storing a matrix of n^2,

36

we need store just three n-dimensional vectors. In summary, by eliminating the unnecessary zero items in the matrix A, TDMA can save computational time and use less system memory, which eventually leads to the improvement of the efficiency.

4. Newton-Raphson Algorithm [35]: Newton-Raphson method is one the most powerful methods in solving the nonlinear equations system. It is a root-finding algorithm that uses the first few terms of the Taylor series of a function $f(x)$ in the vicinity of a suspected root. The Taylor series of $f(x)$ about the point $x=x_0+\varepsilon$ is given by

$$f(x_0 + \varepsilon) = f(x_0) + f'(x_0)\varepsilon + \frac{1}{2}f''(x_0)\varepsilon^2 + ...$$

Keeping the term only to the first-order, the above equation can be simplified as:

$$f(x_0 + \varepsilon) \approx f(x_0) + f'(x_0)\varepsilon$$

in which, ε means the offset between the root and an initial guess values x_0. For a given initial guess value x_0, ε_0 can be estimated as $\varepsilon_0 = -\dfrac{f(x_0)}{f'(x_0)}$. After that, the method refines the guessed value as $x_1 = x_0 + \varepsilon_0$, and uses this value

37

to get another ε_j. So on and so forth, the algorithm repeats the same process until it converges to a root using $\varepsilon_n = -\dfrac{f(x_n)}{f'(x_n)}$.

In this study, iterative methods are chosen to solve the differential equations because of the advantage of iterative methods - only non-zero coefficients of the equations are stored in core memory. The mathematical model is implemented in a Java program on the Sun Solaris platform. The program includes three loops. The outer loop adopts Gauss-Jacobi method to solve the equations, such as mass of hydrogen, mass of oxygen, pressure drop, stream temperatures, mass of water vapor and liquid water, and so on. In the inner loop, the Tri-Diagonal Matrix Algorithm is used to calculate the energy balance to get the stack temperature. For the non-linear algorithm equation, such as cell potential – current density equation (51), the Newton-Raphson method is applied to calculate the local current density.

5.2 Discretization

Before the iterative methods can be applied, the differential equations are required to be discretized into algebraic equations. The common discretization methods are finite difference method, finite element method and finite volume method which is also called control-volume-based finite element method [36]. The finite difference method requires the domain to be replaced by a grid. At each grid point, each term in the governing equation is replaced by a difference formula which may

38

also include the values of neighboring grid points. By substituting the difference formula into the equations, a difference equation is obtained. The finite-element method subdivides the calculation domain into elements. The discretization equations are usually derived by the use of a variation principle. In the derivation, a "shape function" or profile assumption is used to describe how the dependent variable varies over an element. For the control-volume-based finite element method, the control volumes are constructed by joining the centroid of each triangle to the mid-points of the sides of that triangle. The discretization equation is formed by adding the contributions of these elements to the integral conservation for the control volume.

In this simulation, the finite difference method is adopted. The channel is subdivided into n control volumes of equal length $L=L/n$ in x direction (Shown in Fig. 4). The exit values at the kth control volume are the inlet values at the $(k+1)^{th}$ control volume, and all variables are stored at the centroid of each cell. A set of differential equations is replaced by algebraic equations based on this method.

5.3 Simulation Procedure

The mathematical model is implemented in a Java program on the Sun Solaris platform. The whole iteration process is divided into two levels: the inner iteration is used to derive the parameters in each control volume, such as, N_{H2}, N_{O2}, N_{N2}, N_{vapor}, N_{liquid}, T_A, T_C, T_S, dp, V_A, V_C, and so on. The outer iteration is used to calculate the parameters in the whole channel, such as, $I(x)$, V_{cell}, P_{in}, $T_{S,in}$, $T_{S,out}$.

39

Firstly, a given value of average current density, I_{avg}, is provided to the simulation process as the initial parameter. Based on this given value of I_{avg}, the flow rates for hydrogen, air and water vapor and liquid at inlet are calculated as initial conditions. In the outer iteration, the guessed value for the cell voltage, the inlet pressure P_{in}, inlet stack temperature $T_{S,in}$ and outlet stack temperature $T_{S,out}$ are chosen. Using the iteration method, the system will calculate a new group of I'_{avg}, P'_{in}, $T'_{S,in}$ and $T'_{S,out}$, which will be used as the updated guess values. The iteration will not stop until the relative errors of I_{avg}, P_{in}, $T_{S,in}$ and $T_{S,out}$ are less than 0.0001 at the same time. During the iteration process, if the relative errors of P_{in}, $T_{S,in}$ and $T_{S,out}$ do not fall into this range, the program will take another group adjusted values P_{in}, $T_{S,in}$ and $T_{S,out}$ as the new input. However, if the relative error between the calculated I'_{avg} and the given I_{avg} is smaller than the specified the convergence criteria, the system will adjust the cell voltage for a new iteration process.

In the inner iteration, initial guessed exit temperatures of flow and exit pressure of the each control volume are chosen. The computational results include: the exit flow temperatures T_A and T_C, pressure drop in each control volume and a set of local current densities which are used to calculate a new I_{avg} in the outer iteration. If the relative errors of T_A, T_C and dp are not smaller than the specified convergence criteria, e.g. 0.0001, the iteration continues with new guess values of T_A, T_C and dp. The flowchart diagram of the algorithm is shown in Fig. 5

40

5.4 Parameters Used in Simulation

In this simulation, the hydrogen and air flow in the channels are in the coflow mode. Table 1 lists the basic geometry parameters and property of electrode and membrane of the unit fuel cell.

6. MODEL VALIDATION AND RESULTS ANALYSIS

Choosing the right modeling parameters is essential in establishing the base case to validate the simulation results against experiments. Most current theoretical and experimental research of the PEM fuel cell only focus on the high temperature and high pressure operating environments. For low temperature and low pressure operating conditions, experimental results are hardly available from the literature. To verify the effectiveness of the simulation model, the simulation results under low temperature and low pressure conditions are compared with the experimental data obtained from a Ballard Nexa™ Power Module, which operates at room temperature and room pressure with maximum power output 1.2 KW. In this section, the simulation model is verified firstly. Then the simulation results from the base case is analyzed and the most important factors which affect the performance of PEM fuel cell are considered.

6.1 Validation of the Model

The experiment is performed by Dr. Andrzej Sobiesiak's team in University of Windsor and the Nexa™ system is used in this experiment. The Nexa™ system [37] consumes hydrogen and air to provide DC power up to 1200 watts with a nominal output voltage of 26 VDC. It contains a BALLARD® fuel cell stack, as well as all the auxiliary equipment necessary for fuel cell operation. Auxiliary subsystems include hydrogen delivery, oxidant air supply, cooling system and operational safety systems

for indoor operations. The onboard sensors monitor the system operations and records the experimental data. All operations are automatically controlled by the microprocessor and the control board.

Fig.6 compares the simulation results for constant stack temperature and for variable stack temperature with the experimental data. When the current density is less than 0.25 A/cm^2, the output voltage in the modes is greater than the experimental results. After the current density exceeds 0.3 A/cm^2, the output voltage in the model is less than the experiment results. Obviously, the inner resistances in the models are greater than that in practice. Meanwhile, the resistance in the constant stack temperature model is greater than that in the variable stack temperature model. It is difficult hard to explain clearly the exact reasons for the errors between the model results and experiment results. However, some factors may contribute to the error of the resistance calculation, which lead to the above simulation result.

In the model, $\dfrac{I(x)t_m}{\sigma_m(x)}$ represents the ohmic loss inside the fuel cell, which depends on local current density, membrane thickness, and the membrane conductivity. The experimental equation for membrane conductivity comes from experiment [38], which is based on a fully hydrated membrane of Nafion 117. In the real situation, at many local points of membrane, the hydration is not perfect, which means the water activity in membrane is varied. In additional, the Nexa^{TM} power module didn't provide material and thickness of the membrane. According to previous research [39], the material and thickness of the membrane affect the membrane

43

conductivity greatly. Without the detailed information regarding the membrane, it is hard to obtain very agreeable curves between model results and experimental results. Similarly to the above explanation, the single cell is assumed to be cooled on the both sides. In the Nexa^{TM} power module, several single cells are cooled together as a stack. Thus, the temperature for each single cell in the stack is higher than that in the model. As we know, the higher stack temperature will lead to higher saturated pressure and a lower water activity, which means the membrane conductive becomes lower and the resistance is higher than those in the model.

From the above analysis, it is obvious that modeling the ohmic loss inside a PEM fuel cell is not an easy task. When the experimental facility has a complex structure and information such as the membrane resistance is not available, some adjustments seem to be necessary. Considering all the above factors, it is possible that the experimental equipment has a lower membrane resistance than our model. By multiplying a coefficient, which is less than one, with the ohmic loss item in the equation, we get a new curve which is plotted in Fig. 7. As we can see, this adjustment produces a better simulation result and the slope of this curve is closer to that of the experiment data. In order to get a more matched simulation result with the experiment, it is necessary to improve the model of the membrane resistance based on each specified experimental environment. Nevertheless, in this research, the current model is used for further discussion since its simulation follows the same trend as the experimental data and have an acceptable accuracy at the same time.

44

6.2 Grid Study

The convergence behavior and accuracy of a numerical solution depends on the grid quality. In general, a finer grid provides more accurate solution, however, it will require more computer memory and computational time. Whereas, the larger grid can increase the efficiency of the computational process, but, it cannot provide a very accurate solution. Therefore, it is important to find the grid size that provides the accuracy and efficiency needed for the simulation. In this study, the number of mesh has been compared as 100, 300 and 500 cells. The simulation results for 100 and 300 have some difference. However, there is no significant difference between the simulation results for 300 and 500 cells. Considering the increase in computational cost for the finer mesh, the mesh of 300 cells is chosen in this study.

6.3 Base Case Analysis

The simulation is based on an operating condition at near room temperature and low pressure, which is called the "Base case". The detailed operating conditions of the base case are listed in Table 2.

Fig. 8 shows the local current density in the base case along the channel. The current density is the highest at the inlet of channel. It then drops quickly to the lowest point. After that, current density increases slowly along the channel until it reaches the exit of channel, where the current density increases sharply. This observation can be explained as the water activity in membrane changes along the channel.

45

Fig. 9 shows the water activity in the cathode flow, anode flow and membrane respectively. Near the inlet of the channel, the water vapor in the flow is sufficient and the membrane is well hydrated, which increases the local conductive and electro-osmotic drag coefficient of membrane. As a result, more hydrogen ions can pass through the membrane and generate higher current density. Further down the channel, the water activity at the anode flow drops quickly and the membrane becomes drier and more resistive which decreases the current density. However, since there is some water produced by the electrochemical reaction continually at the cathode, the water activity of the stream increases gradually along the channel. Correspondingly, the current density increases. In summary, the water vapor fraction in the flow has a direct impact on the fuel cell performance. Fig. 9 also displays that the water activity in the membrane depends on the water activity in both cathode stream and anode stream.

Fig. 10 shows how the mole number of oxygen and hydrogen decrease along the channel. Since the excess coefficient of air is higher than that of hydrogen, the molar fraction of oxygen is larger than that of hydrogen at the exit of channel. The reason for choosing a large excess coefficient of air is that the excess air is needed to take away the extra water in the cathode channel. Mole number of nitrogen doesn't change because it is not involved in the electrochemical reaction.

Fig. 11 shows the relationship of water activity, water content and water relative humidity in channels which have been defined in the section of model description. In the cathode channel, the relative humidity of stream is equal to 1.0.

46

Because the water is produced continually, the water activity and water content keep increasing. When the water vapor partial pressure is greater than the saturated pressure, water vapor will condense to liquid water. If the water vapor condensation rate is too low, the water vapor partial pressure can be greater than the saturated pressure in a short period. Therefore, the water activity can be greater than 1.0. According to their definitions, the difference between the water activity curve and water content curve at some point indicates that there is liquid water in this part of the channel. In the anode channel, since the flow is usually unsaturated and there is no liquid water along the channel, the three curves are overlapped. Fig. 12 shows the relationship between water content and water activity when the anode inlet water content is 1.25 and the liquid water is injected into the anode channels. In this special case, although relative humidity along the channels is no more than 1.0, it still can be seen that the water content curve and water activity curve are not overlapped. The area between water content and water activity means that liquid water exists in the channels. This phenomena is due to the lower liquid water evaporation rate. Meanwhile, it is found that the water content curve and water activity curve overlap after 60% of the channel length. This behavior is attributed to the fact that all of the liquid water evaporates into water vapor at the point of 60% of the channel length. Beyond this point, there is no liquid water in the channel.

Fig. 13 shows the temperature distribution of the cathode stream, the anode stream and the stack along the channel. Fig. 14 gives the detailed temperature curves in the vicinity of the inlet. At this part of the channel, heat can be transferred from the

47

stack to the environment by the convection, which leads to the stack temperature being lower than the stream temperature. Further down to the channel, there are several heat transfer processes taking place: (a) a chemical reaction occurs and reaction heat is released to the solid stack. (b) water vapor condenses and latent heat is released. (c) convection heat transfer occurs as well due to the temperature difference between the stream and stack. According to the curve, the anode temperature drops quickly near the inlet of the channels. When it reaches the stack temperature, it increases with stack temperature. The cathode temperature drops slowly, at 15% of the channel length, it reaches the same temperature as the stack. It can be seen that the large flowrate leads to the flow temperature changing slowly at the cathode.

Fig. 15 shows the distribution of pressure along the channel. Obviously, the pressure drop at the cathode channel is larger than that at the anode channel. This is because the flowrate at cathode increases, which increases the flow velocity as well. On the other hand, the flowrate and velocity of the stream at the anode decreases, consequently, the pressure drop decreases as well.

6.4 Influence of the Inlet Temperatures of Reactant Gases

In this section, the effects of inlet temperatures of flow on the PEM fuel cell performance will be evaluated. The inlet temperatures of flows at both anode and cathode are set to 303 K, 313 K, 323 K, 333 K, and 343 K, respectively.

The distribution of current density with different inlet temperatures is shown

48

in Fig. 16. The distributions of current density are totally different for each inlet flow temperature. When the inlet temperatures of flows are 303 K and 313 K, the values of current densities are highest at the inlet of channel. They then decrease quickly until they reach the lowest point at around the 8% of length down the channel. After that, the current density increases again. The distribution of current density is very interesting when the inlet temperature of flow is 323 K. The current density increases slightly around the entrance, and then begins to drop along the channel. At approximately 10% of channel length, the current density begins reaches the lowest value. After that, the current density turns back to increase again. This upward tendency stops at the position of about 60% of the channel length. When the inlet temperatures of flows are 333 K and 343 K, the current densities increase near the inlet, and then keep decreasing until the exit of channel. This happens primarily because the current density depends on the water activity in the membrane and the partial pressure of oxygen in cathode stream. At a low inlet temperature, since the gas carries little water vapor, water activity is the primary factor that affects the current density.

Fig. 17 shows the distribution of water activity at the different inlet flow temperatures. It is found that the local water activities in the membrane are less than 1.0 when the inlet flow temperatures are 303 K and 313 K. At a position around the 8% of the length down the channel, the water activity in the membrane reaches the lowest point. This means the membrane is very dry and the speed of electrochemical reaction is slow. Consequently, only a small number of electrons is produced, which

49

leads to lower current density. With the increasing membrane water activity along the channel, more hydrogen ions pass through the membrane and therefore, the current density increases. It is also noticeable that the membrane activity increases quickly near the exit of channel. This can be explained due to the fact that the stack losses heat to environment, which quickly lows the stack temperature and flow temperatures. According to equation (43), the saturated pressure will drop and the water activities will increase. For the cases with higher inlet temperature, such as, 333 K and 343 K, the gases carry more water vapor into channel. Fig. 17 shows that the water activity in membrane along the whole channel is greater than 1.0. According to equation (53), the membrane conductivity changes are small when water activities are large enough. Thus, membrane is hydrated well and the speed of electrochemical reaction is fast. As a result, more oxygen is consumed and the partial pressure of oxygen decreases quickly (shown in Fig. 18). This effect contributes to the drop of the current density along the channel. When the inlet temperature is 323 K, the current density depends on both membrane water activity and partial pressure of oxygen. From the entrance of channel to about 60% of channel length, the membrane water activity is less than 1.0. The current density changes with the increasing membrane water activity. When the membrane water activity is greater than 1.0, the membrane conductivity doesn't change much. However, the partial pressure of oxygen decreases quickly and consequently, the current density drops beyond 60% of the channel length.

Fig. 19 shows that increasing the inlet temperature of flow yields a higher cell potential. This behavior is attributed to the fact that the flow with high

50

temperature introduces more water into the channel and the membrane resistance decreases due to the hydration. It is noticed that the polarization curves at the inlet flow temperatures of 333 K and 343 K are overlapped. This is because that the membrane resistance remains basically constant when the membrane is hydrated well (water activity is greater than 1.0 along the whole channel).

Fig. 20 shows the stack temperature distributions. It can be seen that the tendency of stack temperature is similar to that of current density. The larger the current density is, the more the reaction heat is released and the higher the stack temperature. Fig. 21 shows that the inlet temperatures of flow have a great effect on the pressure change along the cathode channels. When the inlet flow temperature is high, the speed of electrochemical reaction increases and more air is required. Thus, the flowrate in the cathode channels increase and the pressure drop increases as well.

6.5 Influence of Pressure

Fig. 22 shows how the pressure affects the performance of a PEM fuel cell under various current densities. Over the entire range of the investigated current densities, a higher pressure leads to higher performance of the fuel cell. However, the potential difference between 1 atm and 2 atm is bigger than that between 2 atm and 3 atm. Furthermore, this effect is more obvious when the current density is high. This is because the high-pressure streams can bring more water into the channel (shown in Fig. 23). As a result, the membrane is better hydrated and the speed of chemical

51

reaction increases. Therefore, the fuel cell can generate more power under the high flow pressure. From the above analysis, a conclusion can be drawn that a high inlet gas pressure has a positive effect on the system performance of fuel cell. However, whether to use the high pressure in a real fuel cell design depends on the trade off between the system improvement and the cost of providing compressed gas.

6.6 Influence of Coolant Temperature

Generally, the fuel cell system has cooling equipment to remove waste heat and keep the fuel cell working under optimal conditions. To simulate this kind of situation, it is required to investigate how the coolant temperature affects the fuel cell performance. To keep it simple, the coolant temperature is assumed to be constant. In order to study the effect on heat removal, the polarization curves with different coolant temperature, which are 293 K, 298 K, and 303 K respectively, are plotted in Fig. 24. The operating conditions of the fuel cell are: the flow inlet temperature at 313 K and average current density at 0.45 A/cm^2. As we can see, the lower the cooling air temperature is, the better fuel cell performance can be. The reason behind this phenomenon is quite simple. As the coolant temperature becomes lower, more heat can be taken away from the stack, which reduces the stack temperature. As the stack temperature goes down, so do the flow temperatures due to the intensified heat transfer between them (shown in Fig. 25). As the flow temperature becomes lower, the saturated pressure of water vapor drops which leads to an increase of the water

activities. According to Fig. 26, the water activity in the membrane reaches the highest when the coolant temperature is at the lowest point. Therefore, the membrane is hydrated better and the speed of electrochemical increases. As a result, the performance of the fuel cell is improved as well.

6.7 Influence of Anode Inlet Humidification

The water starvation in anode channel is one of the problems that fuel cell designers have to face. As shown in the base case (Fig. 9), the anode and its interface with the membrane become less hydrated as the flow travels along the channels. This is because that the water vapor at anode is carried away by hydrogen ions and transported into the cathode. One way to solve this problem to inject liquid water into the anode channel. As the flow at the anode becomes unsaturated, the liquid water will evaporate to replenish the water loss. Therefore, the membrane is hydrated well. Fig. 27 is variation of the amount of liquid water along the channel. It shows that the liquid water disappears at about 25% of the channel length when the inlet water content at anode is 1.1. If the anode inlet water content increases to be 1.5, the liquid water will exist in the whole channel. This conclusion can be helpful in choosing the optimal anode inlet water content during the fuel cell design.

6.8 Constant Stack Temperature Case Analysis

In many previous studies, the stack temperature of the PEM fuel cell is

assumed to be a constant. However, this temperature is more likely to be variable in real operation. To investigate how the assumption of the constant stack temperature affects the accuracy of the simulation, we simulate the constant stack temperature case and compared the results with those of previous sections. In this section, the Constant Stack Temperature can be referred to as "CST" while the Variable Stack Temperature is labeled as "VST".

Fig. 28 and Fig 13 show the temperature changes along the channel for CST case and VST case respectively. In CST case, the stream temperature at the anode is the same as the stack temperature, since no reaction occurs and no heat is generated. Most of the reaction heat is taken away by the stream in the cathode channel. Obviously, this case is hardly true in real situations. The curves in Fig. 13 are more complex, since it took the reaction heat into account. Here, the anode stream temperature is also close to the stack temperature, but changes along the channel. As the speed of local reactions changes, the local temperature of the cathode channel changes considerably as well. In other words, the temperature fields of the CST case in both the cathode and anode channels are quite different to those of VST case.

Fig. 28 shows the local current density of the base case along the channel for the CST case. As in the case of the corresponding curve in Fig. 8 for VST case, the current density is the highest at the inlet of channel. Then, it drops quickly to its lowest point. After that, current density increases slowly along the channel. Unlike the VST case, there is no sudden increase of current density at the channel exit. This can be explained by water activity changes which have be presented in Fig. 29 for the

54

CST case and Fig. 9 for the VST case. Contrary to the VST case, there is no large increase of water activity at the end of the channel when the stack temperature is constant. Therefore, the current density value doesn't jump at the channel exit since it is directly influenced by the water activity. In summary, the variable stack temperature can significantly affect the flow field and thermodynamic parameters inside the channel. Its influence on flow mode and energy conversion efficiency can hardly be ignored. Also, in the PEM model simulation, choosing a right boundary condition assumption is very important.

The inlet temperatures of flow have an impact on the PEM fuel cell performance. Fig. 31 shows that a higher inlet temperature of flow yields a higher cell potential. As discussed before, this is mainly attributed to the fact that the flow with high temperature introduces more water to the channel and decreases the membrane resistance due to the hydration. The distribution of current density with different inlet temperatures is shown in Fig. 32. It is known that the current density depends on both the water activity in the membrane and the partial pressure of oxygen in the cathode stream. Fig. 33 and Fig. 34 show water activity in membrane and the partial pressure of oxygen along the channel. At low inlet temperature, since the gas carries little water, the membrane is dry and the speed of electrochemical reaction is slow. As a result, a small amount of oxygen is consumed and the partial pressure of oxygen is high. When the stream moves down the channel, more water is produced and the membrane is hydrated, which increases the water activity as well as the speed of electrochemical reaction. Therefore, the current density increases in the later part of

55

channel. At high inlet temperature, sufficient water has been carried by the gas at the initial phase and the speed of electrochemical reaction is fast. As a result, more oxygen is consumed and the partial pressure of oxygen decreases quickly. Eventually, these factors lead to the slow down of the electrochemical reaction and decrease of the current density throughout the rest of the channel. Since the simulations provide different flow and temperature fields inside the fuel cell channels for the CST and VST, the reaction speed and the amount of water produced are quite different at each point of in channel. Fig. 31 and Fig. 19 are the polarization curves for the CST case and VST case respectively. In Fig. 31, the difference between high temperature curves, such as 333 K and 343 K, is more obviously than for the low temperature (313 K and 323 K). On the contrary, the low temperature difference is larger than high temperature in Fig. 19. This means, assuming a constant stack temperature not only affects the analysis of flow conditions, it also changes the simulation result of fuel cell performance.

Since a variable stack temperature more likely happens in a real fuel cell, it makes sense to replace the constant stack temperature assumption with a variable stack temperature. Actually, this was shown in the experimental data. In Fig.6, the experimental result has been compared with both the CST case and VST case. It is obviously that the VST case provides a better simulation result.

56

7. CONCLUSIONS AND RECOMMENDATIONS

7.1 Conclusions

In this research, a model of a single PEM fuel cell has been developed. The simulation based on this model can be used to analyze the water transport across the membrane, the water phase-change effect, the pressure variation along the channel and the energy balance. It can also be used to predict the characteristics of the flows inside the channel and analyze the factors that affect the fuel cell performance. Based on this study, the following conclusions can be drawn:

1. The VST model is more accurate than the CST model when predicting a single fuel cell performance.

2. The humidification of both anode and cathode sides is very important factor affecting the performance of a PEM fuel cell.

3. Increasing the flow inlet temperatures is an approach to overcome the water starvation problem. However, if additional equipment is added, the cost of the fuel cell needs to be considered as well.

4. Increasing the flow pressure can improve the fuel cell performance.

5. Proper liquid water injection at the anode channel inlet can be useful in fuel cell performance improvement. An optimal amount of liquid water could be determined using by the simulations based on the model developed in the present study.

57

6. Decreasing the cooling temperature is helpful in improving the fuel cell performance.

7.2 Recommendations for Future Work

It is recommended that future work be conducted:

1. A better empirical equation for the membrane conductivity should be adopted in this model.

2. In order to make the model more accurate, the constant coolant temperature should be replaced by a variable temperature.

3. Two-phase flow can be introduced into this model to more precisely simulate the phase change.

REFERENCES

1. Kenny, Michael, Presentation at the Fuel Cell Vehicle Technology Conference, UC Davis, Davis, CA, 1998.

2. A. Bauen, and D. Hart, Assessment of environmental benefits of transport and stationary fuel cells, Journal of Power Sources, 86 (2000) 482-494.

3. CARB, Proposed Amendments to the California Zero Emission Vehicle Program Regulations, (2000).

4. T. Woegerer, Research, design and construction of proton exchange membrane fuel cell. E.S.419-Project report, the University of Western Ontario, (1998).

5. P. Badrinarayanan, PEM fuel cell water and thermal management: a methodology to understand water and thermal management in an automotive fuel cell system. Birla Institute of Technology and Science, Pilani, India, (1999).

6. J. Larminie, A. Dicks, A fuel cell systems explained, second edition, ISBN: 0-470-84857-X, (2003), 48-75.

7. A. Eggert, P. Badrinarayanan, D. Friedman and J. Cunningham, Water and thermal management of an indirect methanol fuel cell system for automotive applications, Proc. of the 2000 ASME International Mechanical Engineering Congress and Exposition - Heat Transfer Division, 1 (2000), 35-42.

8. M. Fronk, D. Wetter, D. Masten, and A. Bosco, PEM fuel cell system solutions for transportation, Fuel Cell Power for Transportation 2000, Proc. Of SAE 2000 World Congress, (2000) 101-108.

9. K. Prater, Polymer electrolyte fuel cells: A review of recent developments, Journal of Power Sources, 51 (1994) 129-144.

10. P. Costamagna and S. Srinivasan, Quantum jumps in the PEMFC science and technology from the 1960s to the year 2000 Part II. Engineering, technology development and application aspects, Journal of Power Sources, 102 (2001) 253-269.

11. K. Yao, K. Karan, K. McAuley, P. Oosthuizen, B. Peppley, and T. Xie, A review of mathematical models for hydrogen and direct methanol polymer electrolyte membrane fuel cells, Fuel Cells, 4 (1-2) (2004) 3-29.

12. Bernardi, Dawn, Water balance calculations for solid polymer electrolyte fuel cells, Journal of the Electrochemical Society, 137 (11) (1990) 3334-3350.

13. D. Bernardi, M. Verbrugge, Mathematical model of a gas diffusion electrode bonded to a polymer electrolyte, AIChE Journal, 37 (8) (1991) 1151-1163.

14. D. Bernardi and M. Verbrugge A mathematical model of the solid-polymer-electrolyte fuel cell, Journal of the Electrochemical Society, 139 (9) (1991) 2477-2491.

15. T. Springer, T.A. Zawodzinski and S. Gottesfeld, Polymer electrolyte fuel cell model, Journal of the Electrochemical Society, 138 (8) (1991) 2334-42.

16. T. Springer, M. Wilson, S. Gottesfeld, Modeling and experimental diagnostics in polymer electrolyte fuel cells, Journal of the Electrochemical Society, 140 (12) (1993) 3513-3526.

17. T. Springer, T. Zawodzinski, M. Wilson, S. Gottesfeld, Characterization of

polymer electrolyte fuel cells using ac impedance spectroscopy, Journal of the Electrochemical Society, 143 (2) (1996) 587-599.

18. T. Fuller and J. Newman, Water and thermal management in solid-polymer-electrolyte fuel cells, Journal of the Electrochemical Society, 140 (5) (1993) 1218-1225.

19. T. Nguyen and R. White, A water and heat management model for proton-exchange-membrane fuel cells, Journal of the Electrochemical Society, 140 (8) (1993) 2178-2186.

20. J. Yi and T. Nguyen, An along-the channel model for proton exchange membrane fuel cells, Journal of the Electrochemical Society, 145 (4) (1998) 1149-1159.

21. R. Mosdale, and S. Srinivasan, Analysis and performance and of water and thermal management in proton exchange membrane fuel cells, Electrochimica Acta, 40 (4) (1995) 413-421.

22. J. Amphlett, R. Baumert, R. Mann, B. Peppley, P. Roberge, and T. Harris, Performance modeling of BALLARD MARK IV solid polymer electrolyte fuel cell I. Mechanistic model development, Journal of the Electrochemical Society, 142 (1) (1995) 1-8.

23. J. Amphlett, R. Baumert, R. Mann, B. Peppley, P. Roberge, and T. Harris, Performance modeling of Ballard Mark IV solid polymer electrolyte fuel cell II. Empirical model development, Journal of the Electrochemical Society, 142 (1) (1995) 9-15.

24. C. Marr and X. Li, An engineering model of proton exchange membrane fuel cell

performance, ARI, 50 (1998) 190-200.

25. K. Dannenberg, P. Ekdunge and G. Lindbergh, Mathematical model of the PEMFC, Journal of Applied Electrochemistry, 30 (2000) 1377-1387.

26. K. Hertwig, L. Martens and R. Karwoth, Mathematical modeling and simulation of polymer electrolyte membrane fuel cells, Fuel Cells 2002, 2(2) (2002) 61-77.

27. S. Ge and B. Yi, A mathematical model for PEMFC in different flow modes, Journal of Power Sources, 124 (2003) 1-11.

28. X. Xue, J.Tang, A.Smirnova, R.England, N.Sammes, System level lumped-parameter dynamic modeling of PEM fuel cell, Journal of Power Sources, 133 (2004) 188-204.

29. C. Yunus, B. Michael, Thermodynamics – an engineering approach, fourth edition, IBSN: 0-07-238332-1

30. M.Lampinen, M.Fomino, Analysis of free energy and entropy changes for half-cell reactions, Journal of the Electrochemical Society, 140 (12) (1993) 3537-3546.

31. Boca Raton, Handbook of Chemistry and Physics, 62nd ed. CRC Press, FL (1981)

32. C. Barker, ODE Laboratories: A Sabbatical Project, retrieved April 10, 2005 from San Joaquin Delta College, http://calculus.sjdccd.cc.ca.us/ODE/7-C-3/7-C-3-h.html

33. A. Jungmaier, Model partitioning and communication in parallel simulation of analog circuits using waveform relaxation algorithms, retrieved April 10, 2005 from http://www.exp-math.uni-essen.de/~ajung/diplom/

34. E. Weisstein, Newton's method, retrieved April 10, 2005 from

    http://mathworld.wolfram.com/NewtonsMethod.html

35. A. Depoutre, The 2-D Burgers, retrieved April 10, 2005 from

    Equation http://www.enseeiht.fr/hmf/travaux/CD0001/travaux/optmfn/hi/01pa/h

    yb74/node24.html

36. N. Cetin, retrieved April 10, 2005 from

    http://www.inf.ethz.ch/personal/cetin/thesis/thesis/node19.html

37. NEXAtm power module installation manual, Ballard Power Systems Inc., 2002

38. T. Springer, T. Zawodzinski, S. Gottesfeld, Polymer electrolyte fuel cell model,

    Journal of the Electrochemical Society, 138 (8) (1991) 2334-2342.

39. F. Liu, B. Yi, D. Xing, J. Yu, H. Zhang, Nafion/PTFE composite membranes for

    fuel cell applications, Journal of Membrane Science, 212 (2003) 213-223.
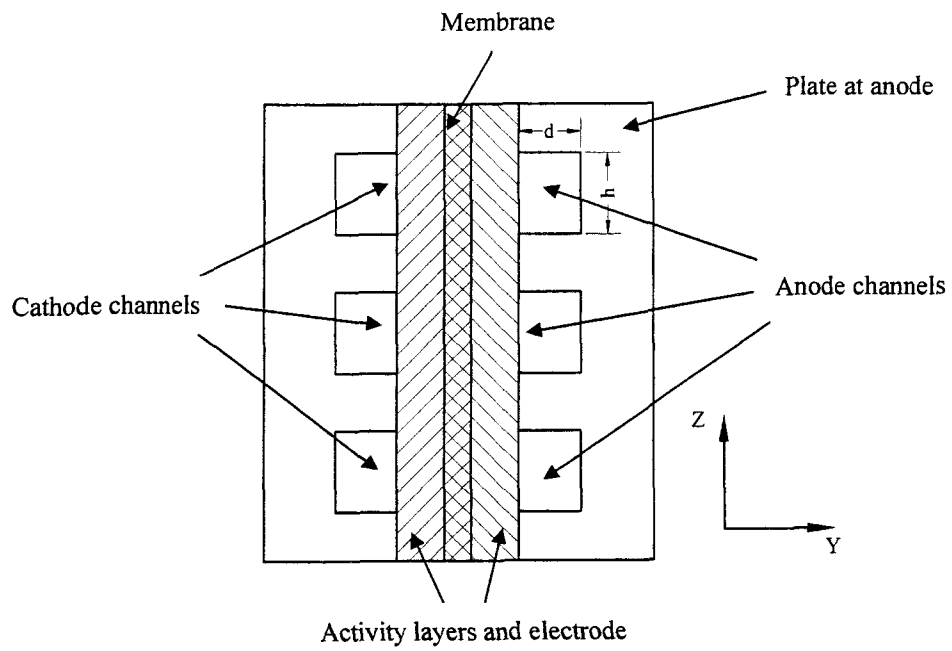
Fig. 1 Schematic diagram of PEM fuel cell modeling regions.

Air, vapor   H2, vapor
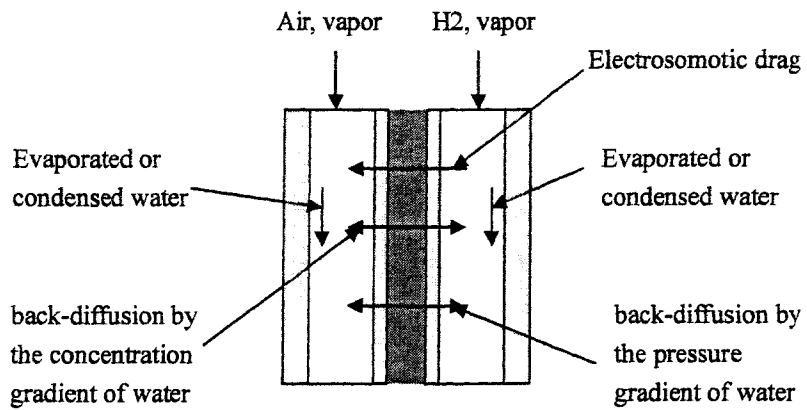
Fig. 2 Mass balance of a unit fuel cell.

Sensible heat at cathode   Sensible heat at anode
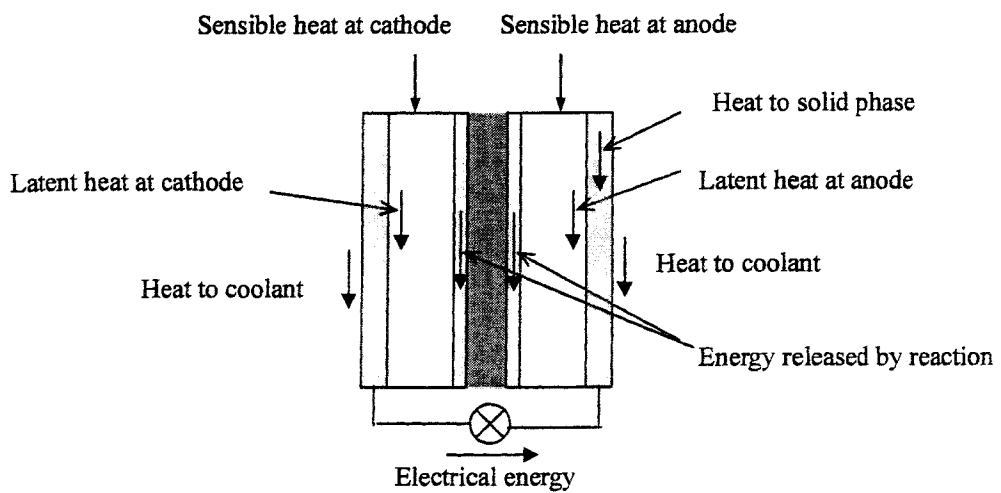
Fig. 3 Energy balance of a unit fuel cell.

65
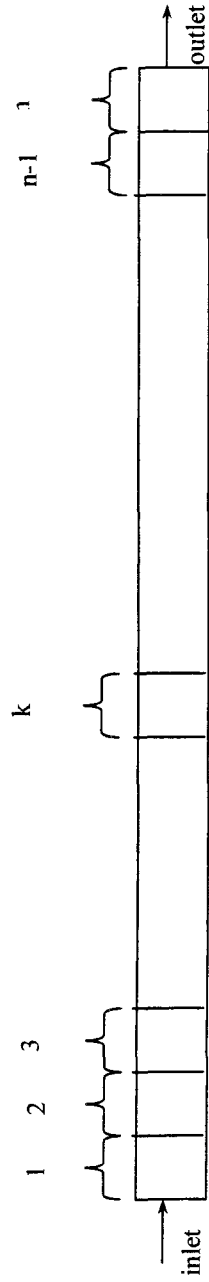
Fig. 4 Control volume layout for numerical solution along the channel.

Guess $p_{\#,in}$ and Guess V_{cell}

Calculate inlet mole number of gases and water

Enter the first control volume ← To next control volume

Guess the pressure drop

Guess stack temperature

Guess temperature of flow

Calculate and get new temperature of flow

$(T_{C\&A,e} - T_{C\&A,e,old}) / T_{C\&A,e,old} < 0.0001$ — N

Y

Calculate and get new stack temperature

$(T_S - T_{S,old}) / T_{S,,old} < 0.0001$ — N

Y

Calculate and get new pressure drop of each control volume

$(dpik_{C\&A} - dpik_{C\&A,old}) / dpik_{C\&A,old} < 0.0001$ — N

Calculate and get the pressure drop of whole channel and new I_{avg}

$$\frac{pik[ns-1]_s - p_{C\&Aout}}{p_{C\&Aout}} < 0.0001 \ \& \ I_{avg} = \frac{1}{L}\int_0^L I(x)dx$$ — N

Y

End

Fig. 5   Flowchart of solution procedure
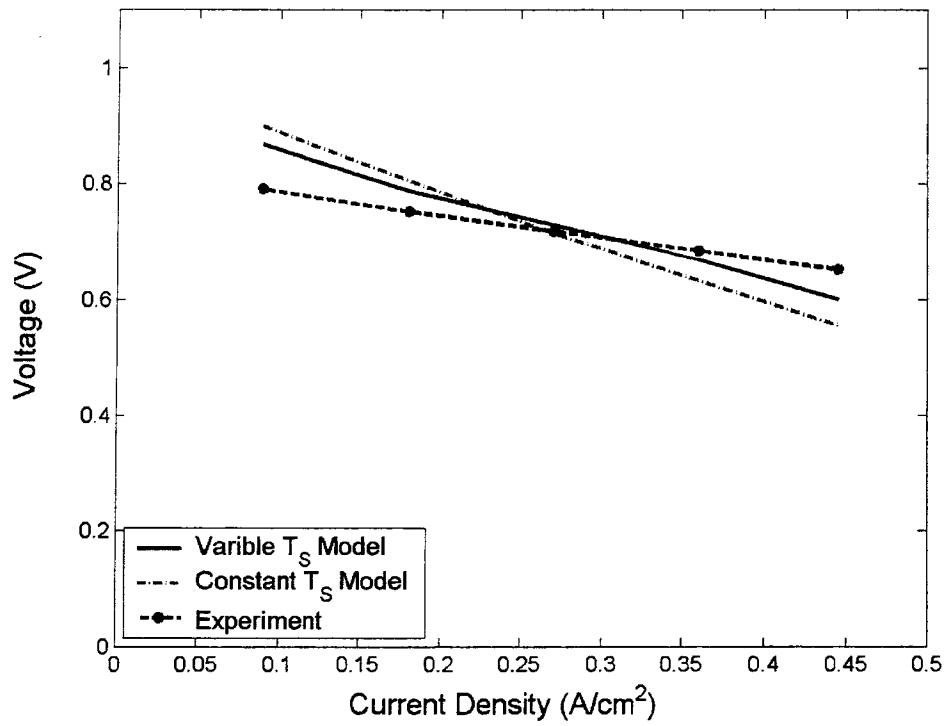
Fig. 6 Comparison of the model predictions with the empirical data
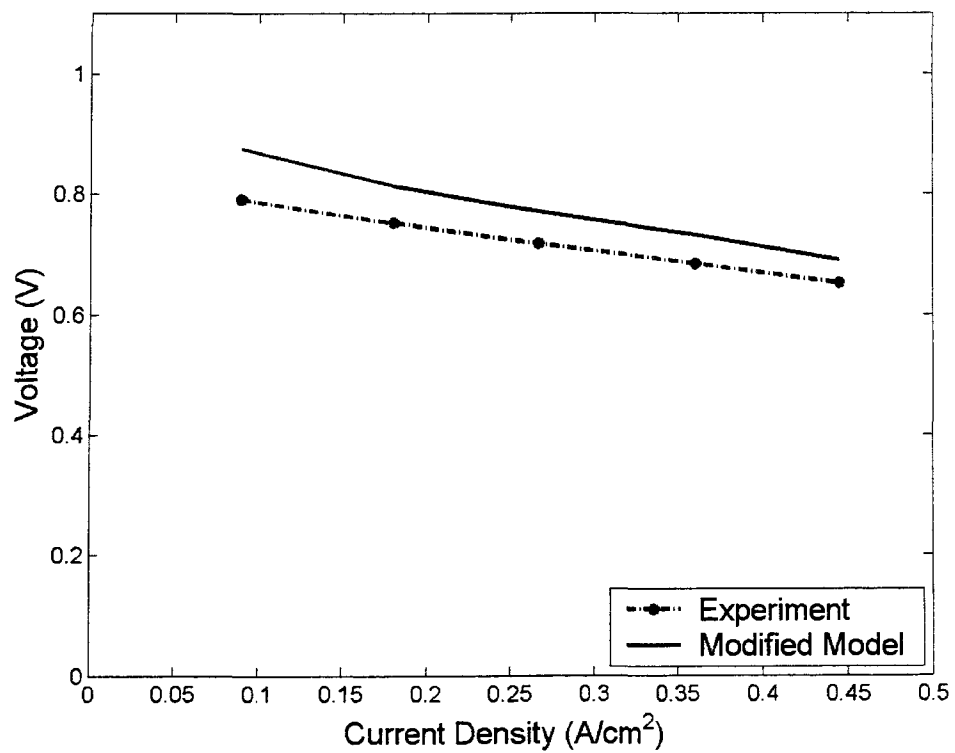
Fig. 7 Comparison of the modified model predictions with the empirical data.
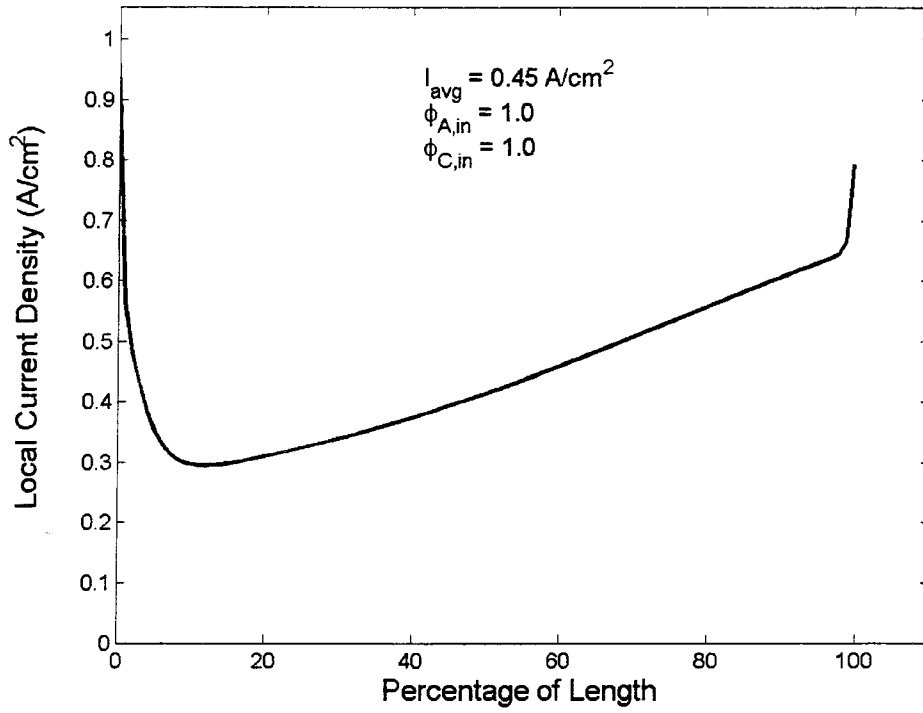
Fig. 8 The distribution of current density along channel in the base case.
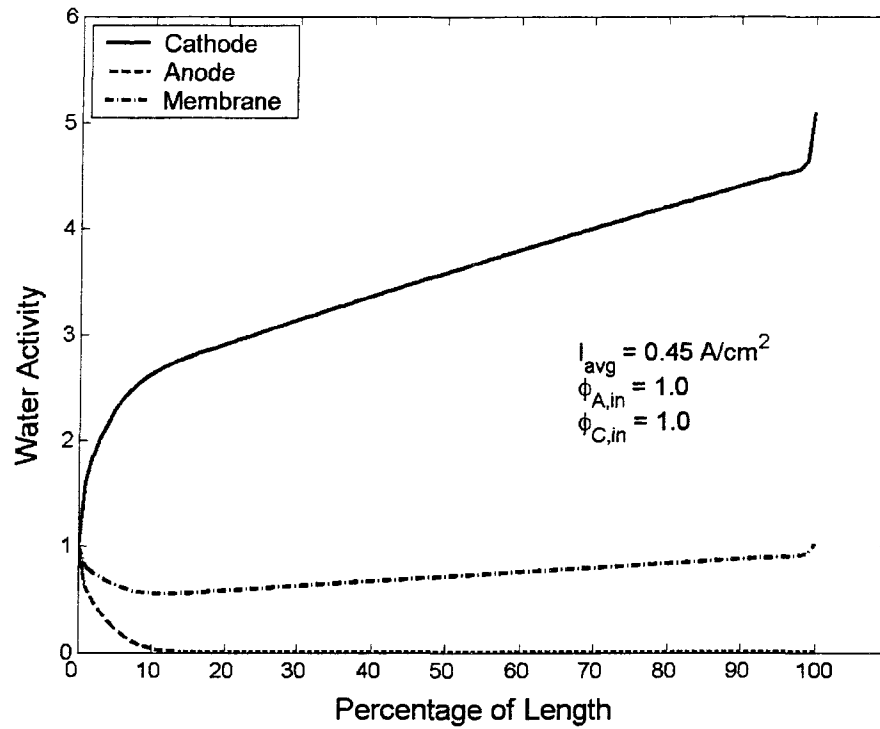
Fig. 9 The distribution of water activity along channel in the base case.
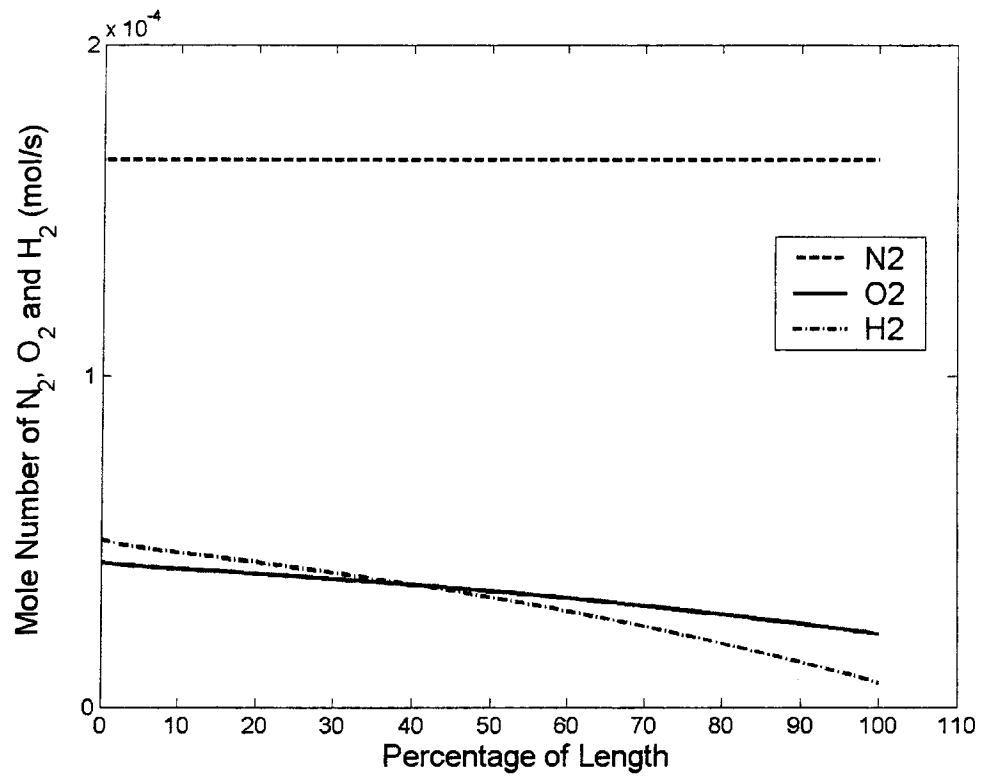
Fig. 10 The distribution of hydrogen, oxygen and nitrogen along channel in the base case.
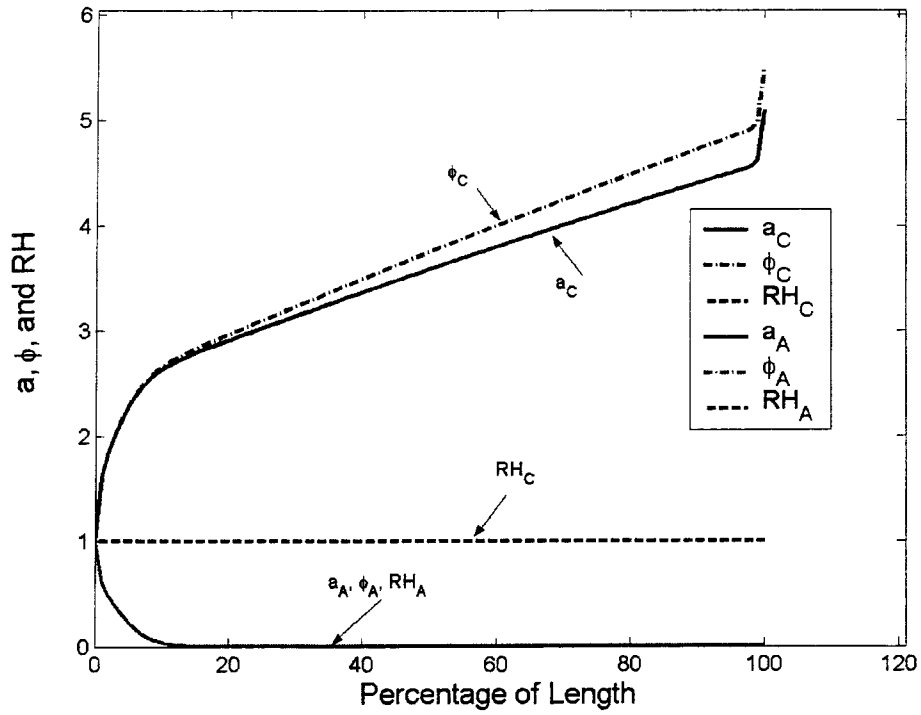
Fig. 11 The water activity, water content and relative humidity along channel in the base case.
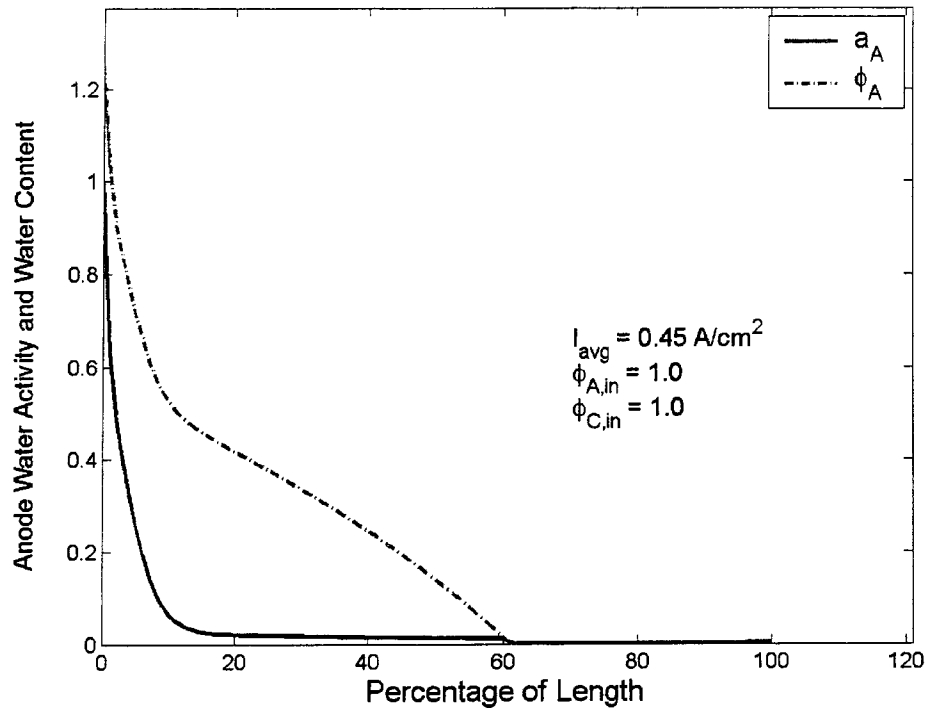
Fig. 12 The water activity, water content along channel for the liquid water injection case.
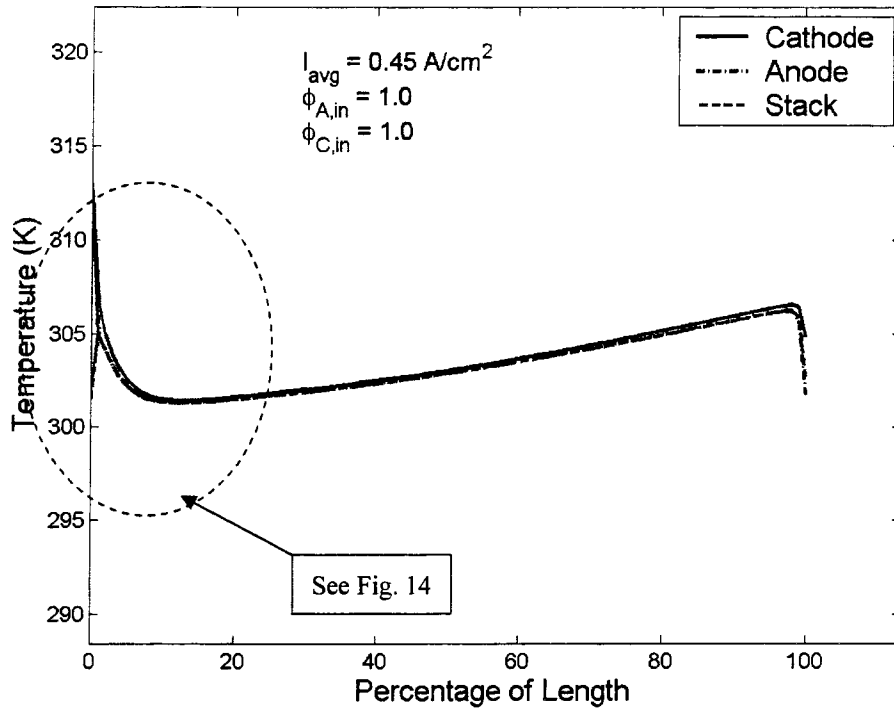
Fig. 13   The distribution of temperature along channel in the base case.
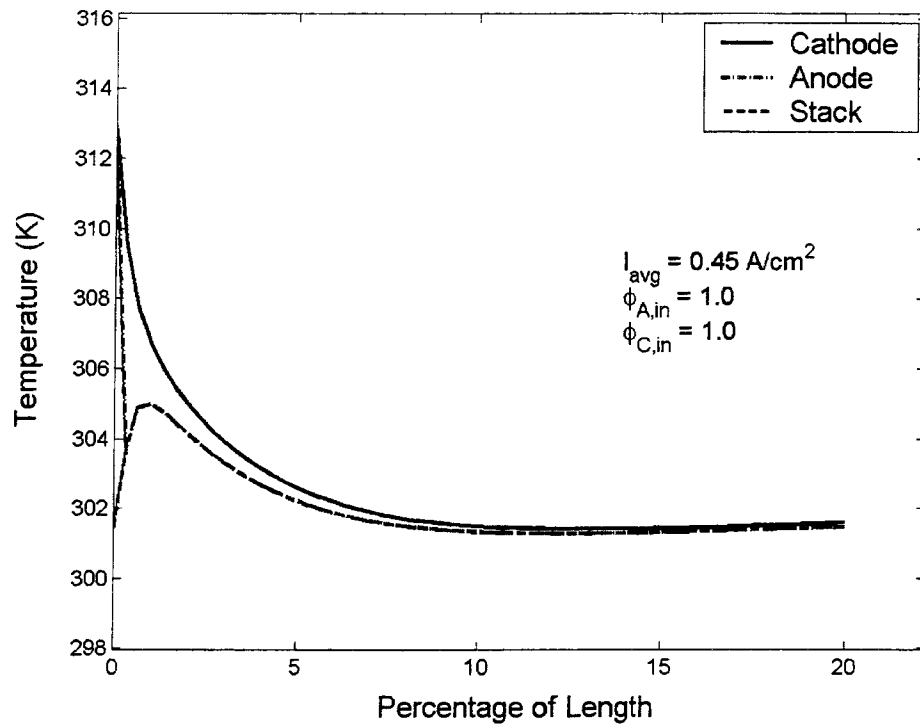
Fig. 14 The distribution of temperature at the inlet of channel in the base case
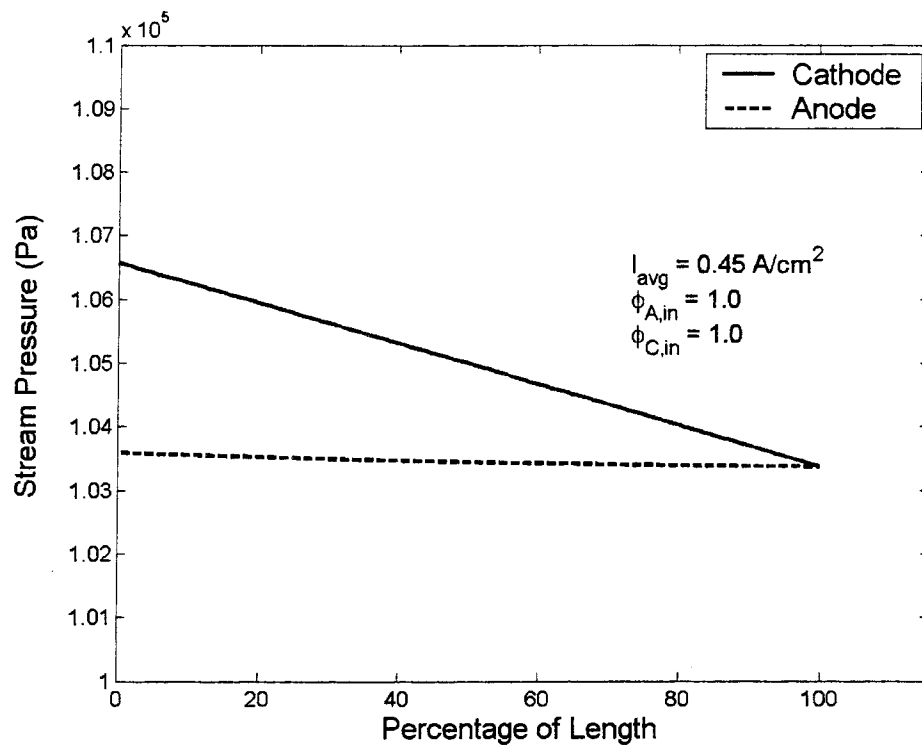
Fig. 15 Distribution of pressure along channels in the base case.
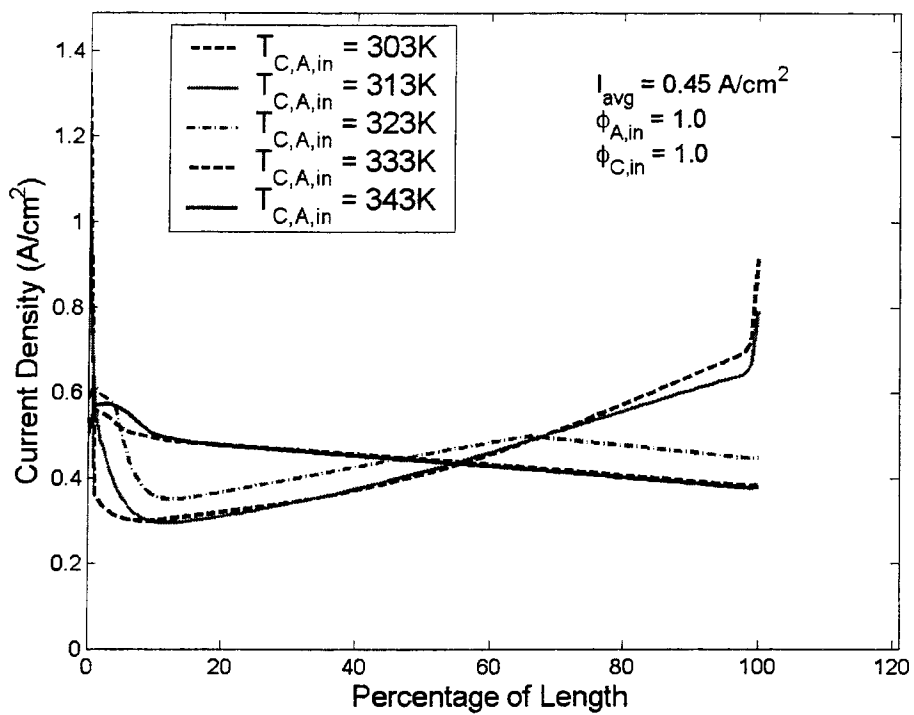
Fig. 16 A comparison of current profiles along the channels with the different inlet stream temperatures.
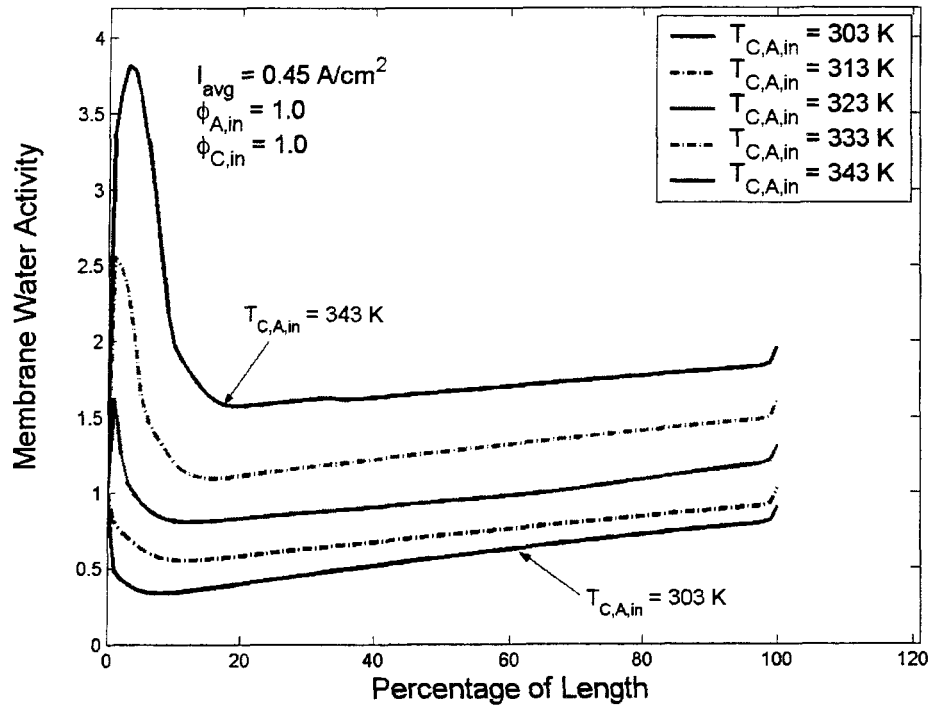
Fig. 17 A comparison of membrane water activity along the channels with the different inlet stream temperatures.
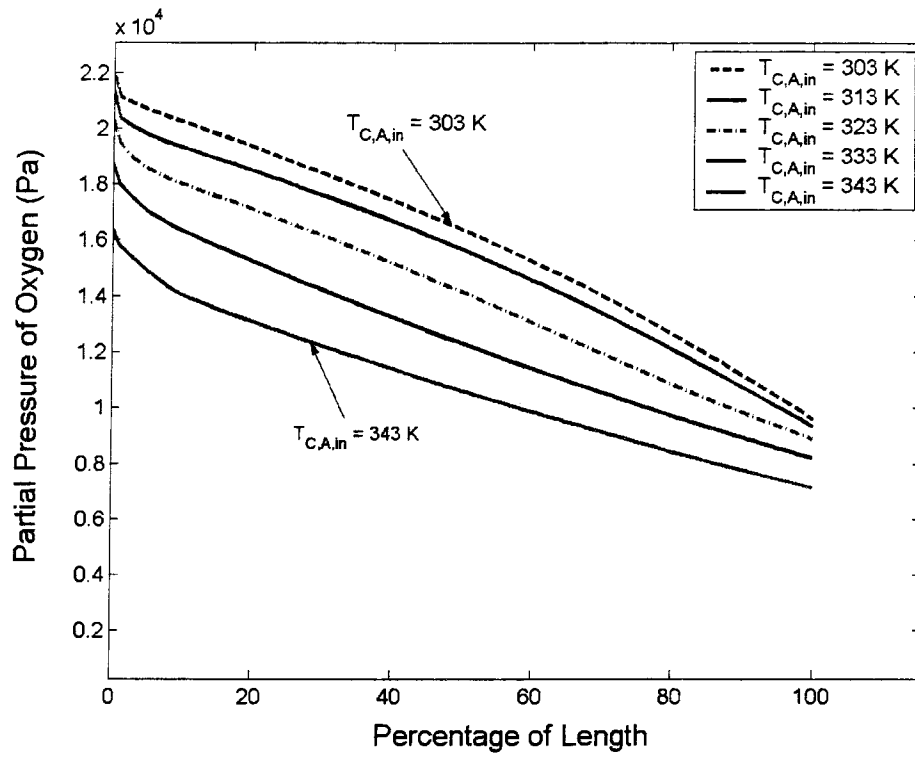
Fig. 18 A comparison of partial pressure of oxygen along the channels with the different inlet stream temperatures.
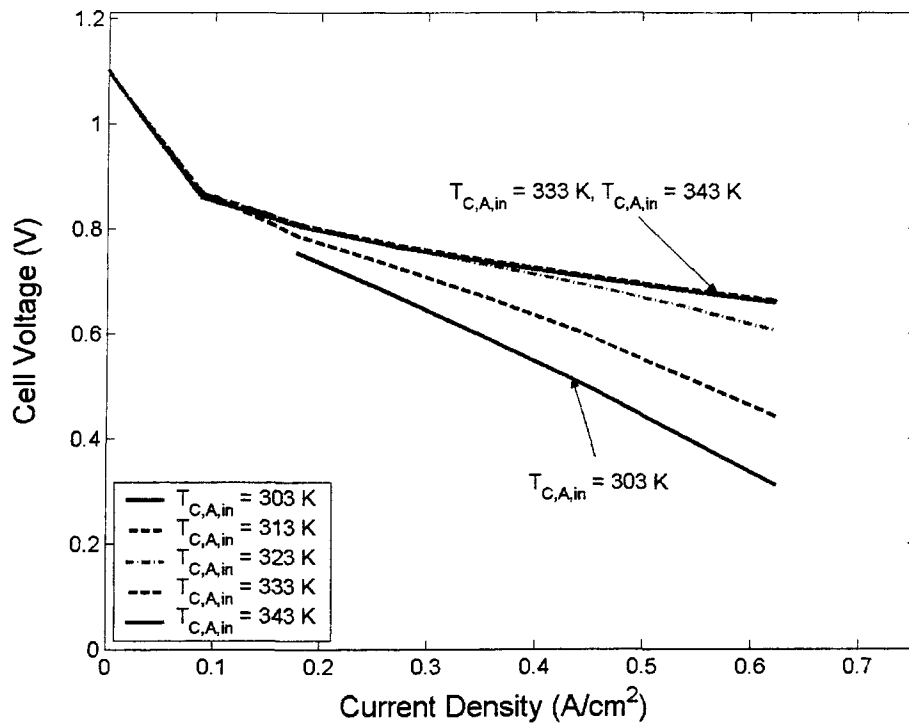
Fig. 19 The effect of inlet stream temperatures on the performance of a single PEM fuel cell.
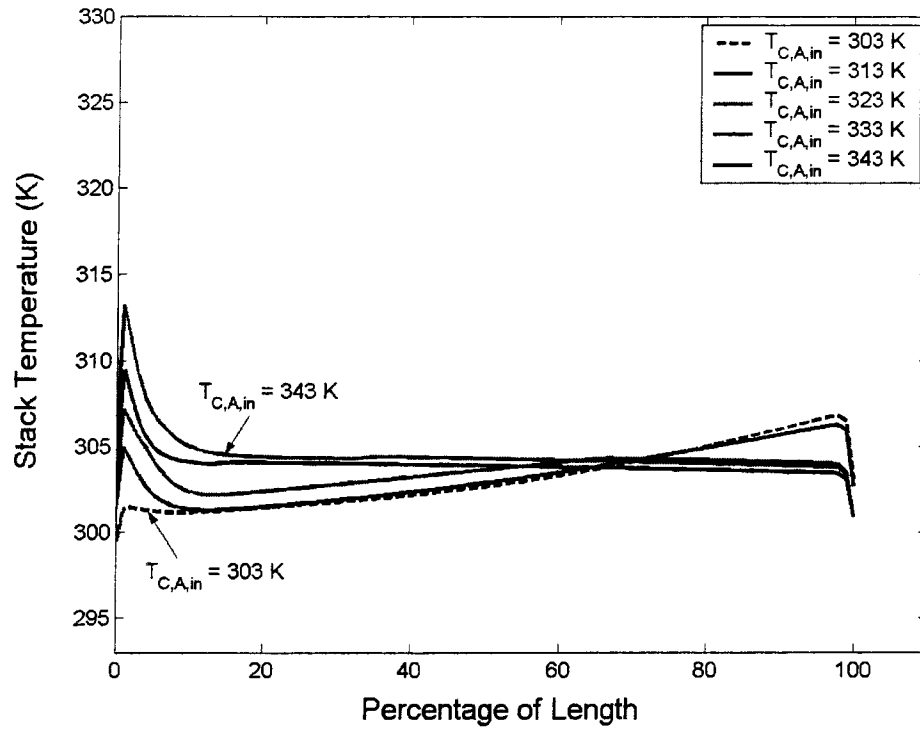
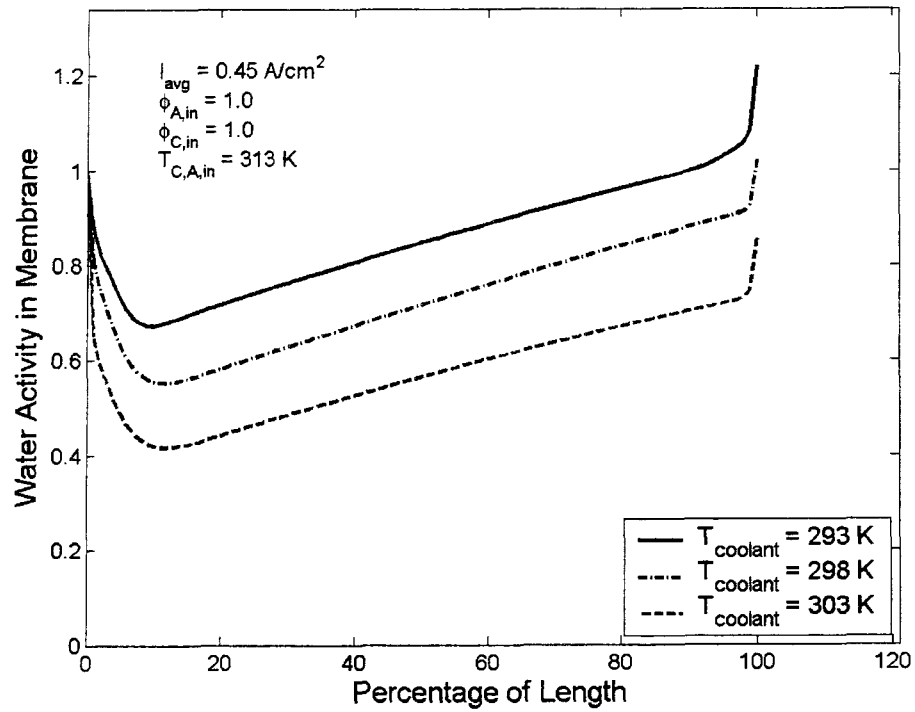Fig. 20 The effect of inlet stream temperatures on stack temperature of a single PEM fuel cell.
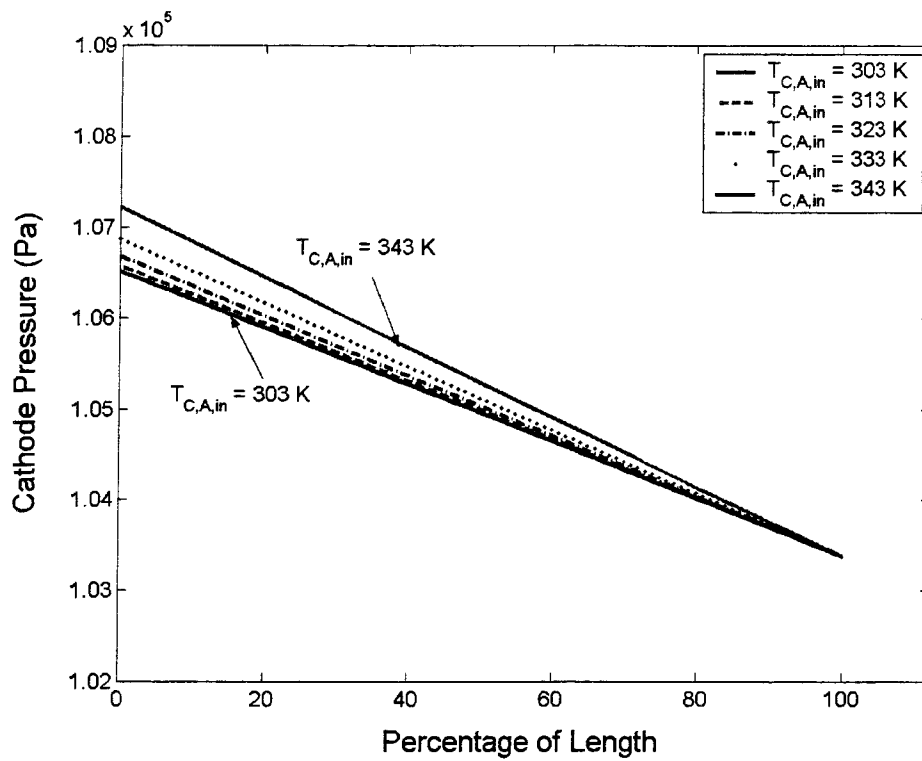
Fig. 21 The effect of inlet stream temperatures on cathode pressure of a single PEM fuel cell.
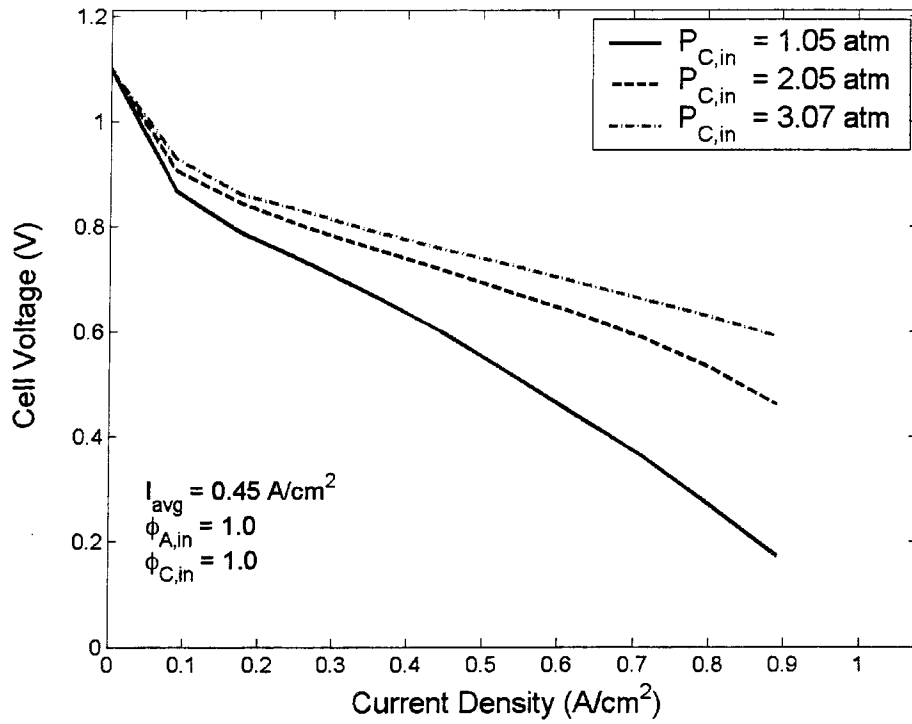
Fig. 22 The effect of pressure on the performance of a single PEM fuel cell.
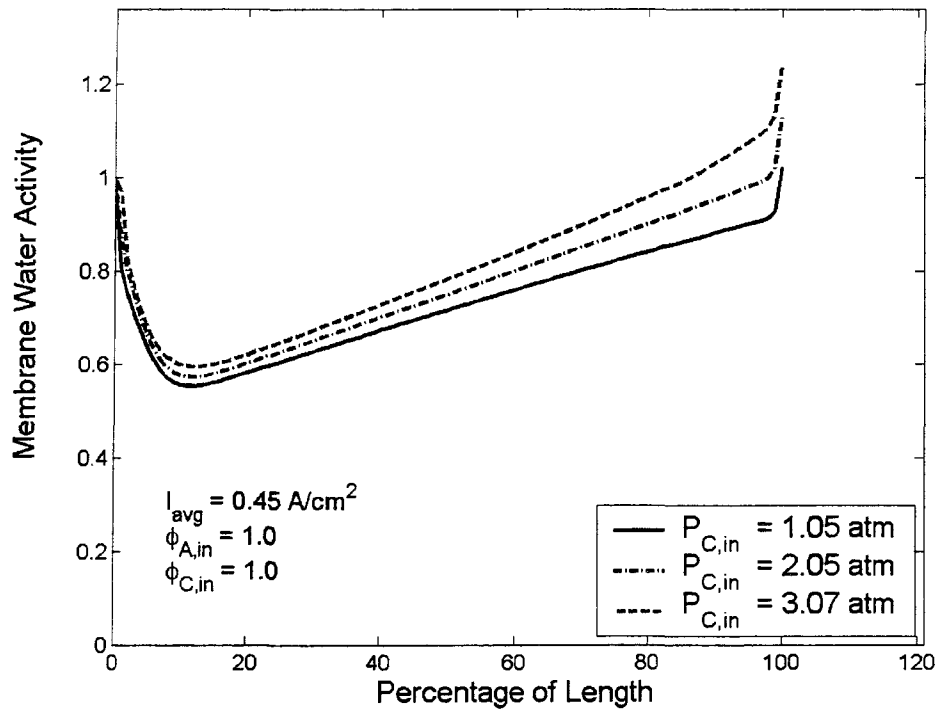
Fig. 23 The effect of pressure on membrane water activity of a single PEM fuel cell.
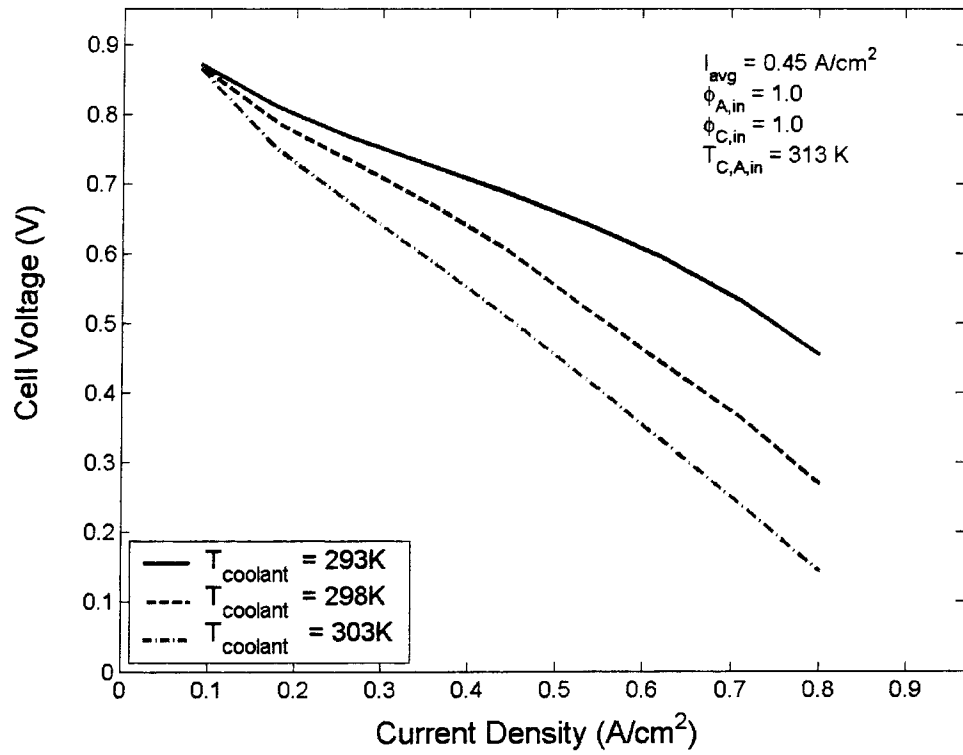
Fig. 24   The effect of coolant temperature on the performance of a single PEM fuel cell.
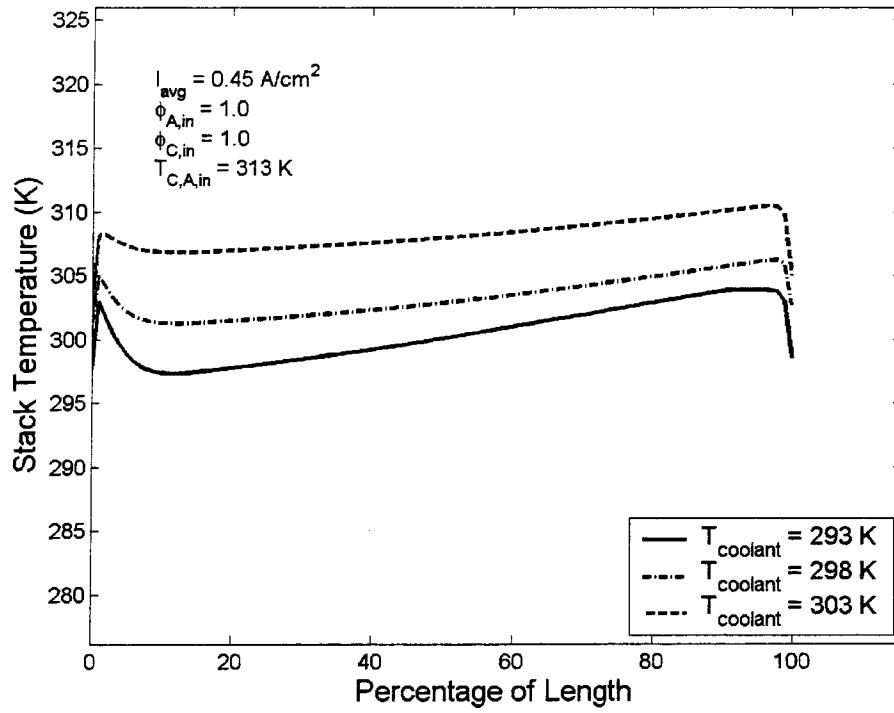
Fig. 25 The effect of coolant temperature on stack temperature of a single PEM fuel cell.

Fig. 26 The effect of coolant temperature on membrane water activity of a single PEM fuel cell.
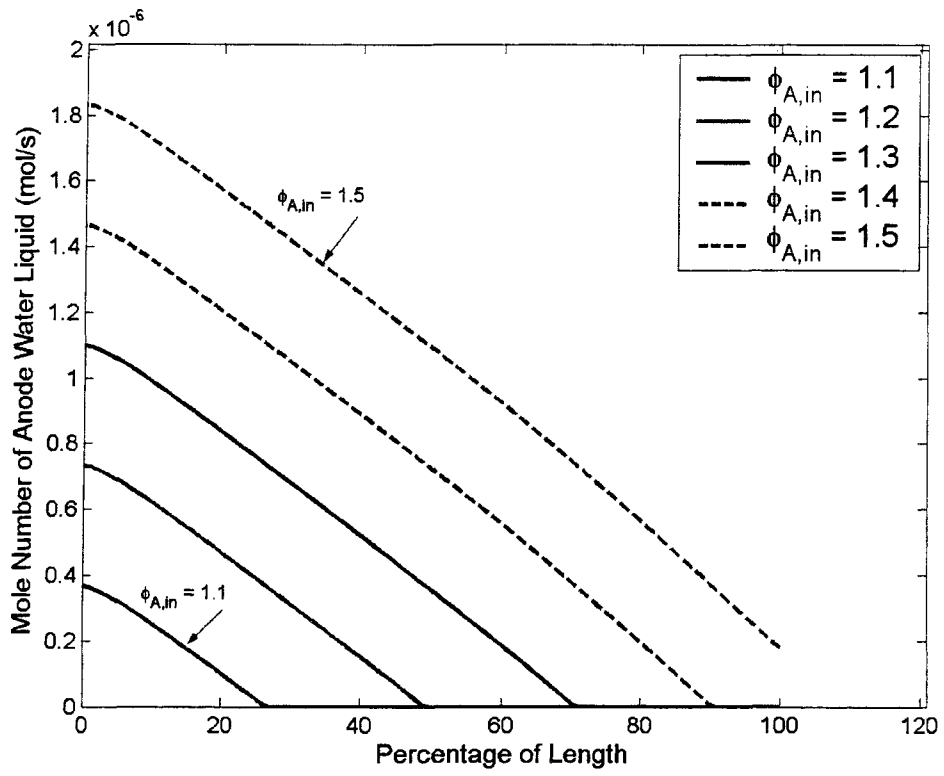
Fig. 27 A comparison of liquid water vary along the channels.
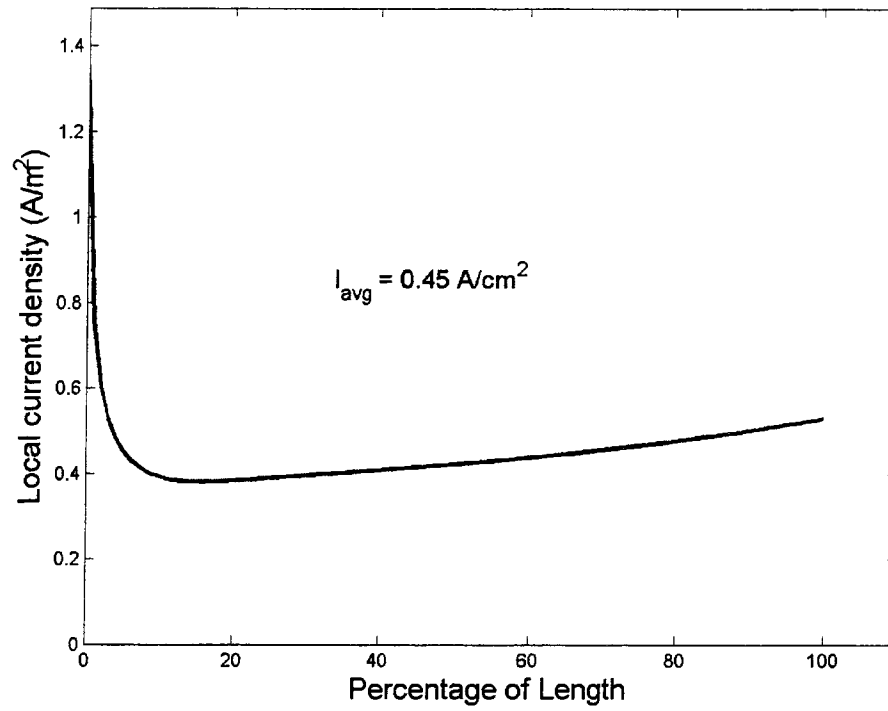
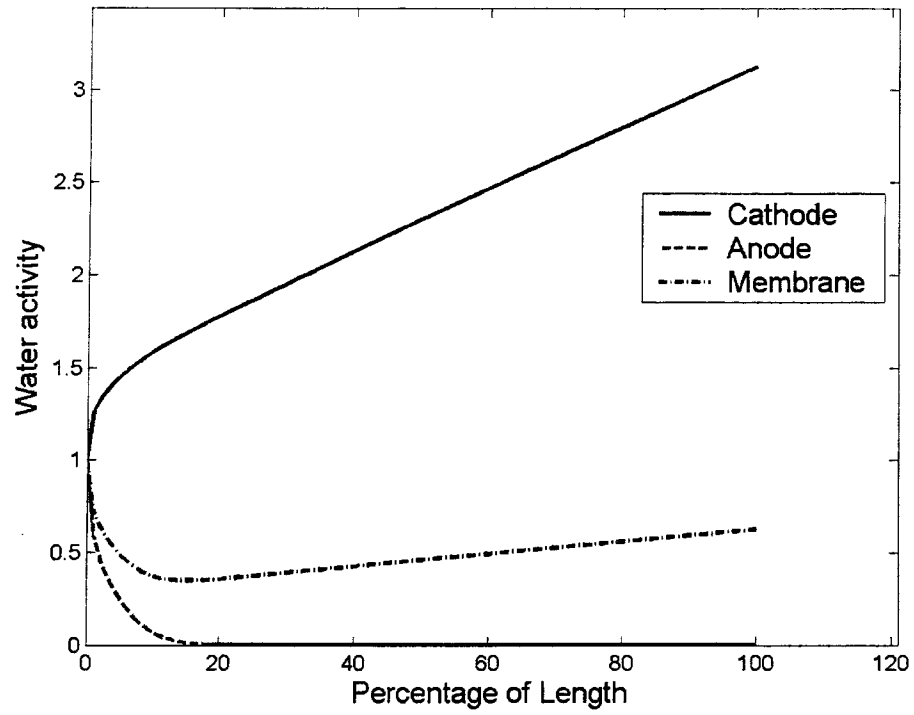Fig. 28 Current density distribution along the channel in the base case of constant stack temperature.

Fig. 29 Water activity distribution along the channel in the base case of constant stack temperature.
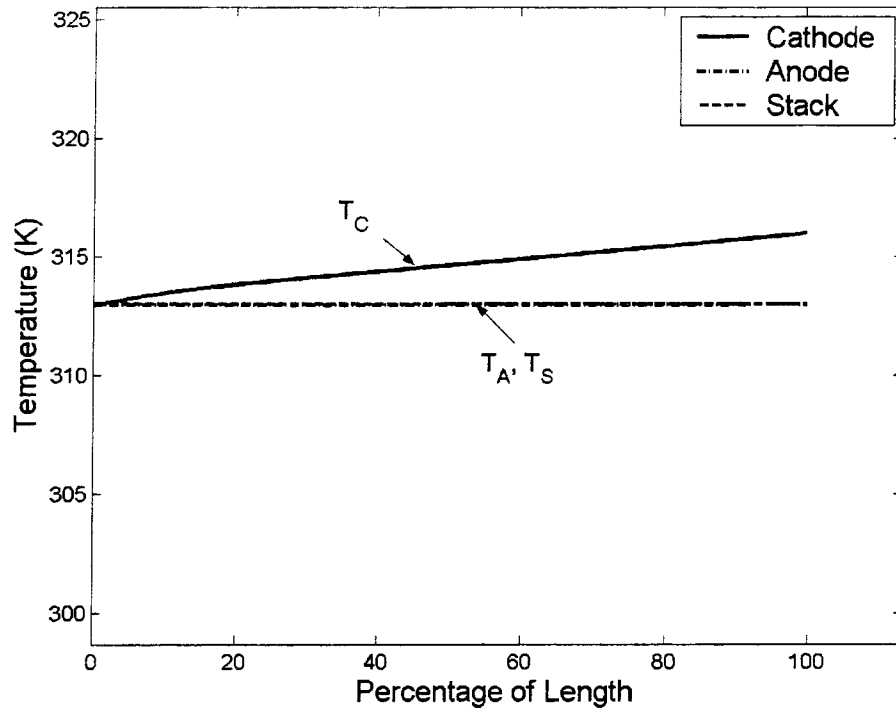
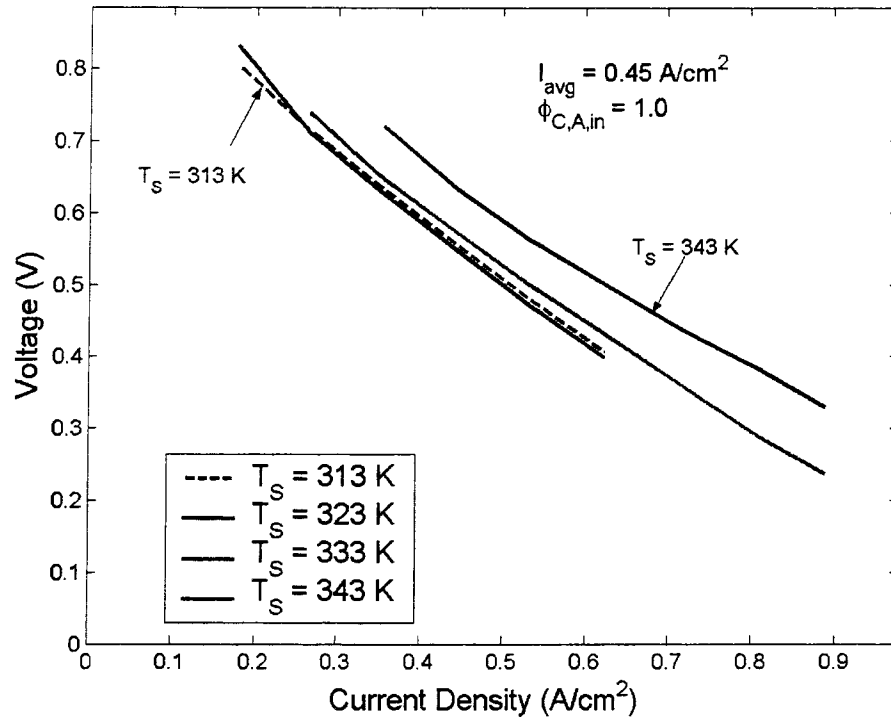Fig. 30 Flow temperatures and stack temperature distribution along the channel.

Fig. 31 Polarization curve for different stack temperature.
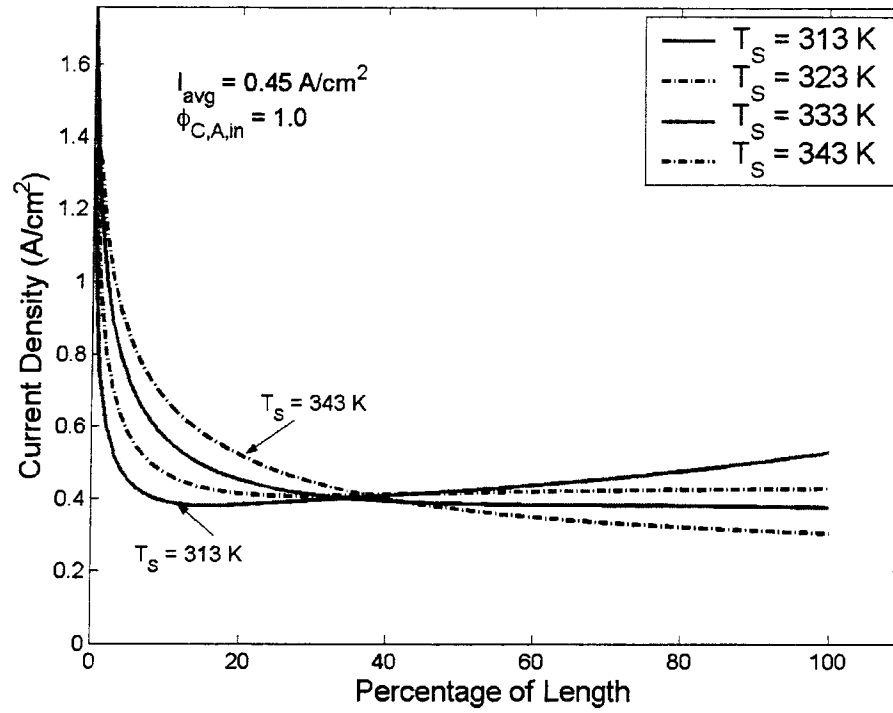
Fig. 32 A comparison of current profiles along the channels with the different inlet stream temperatures.
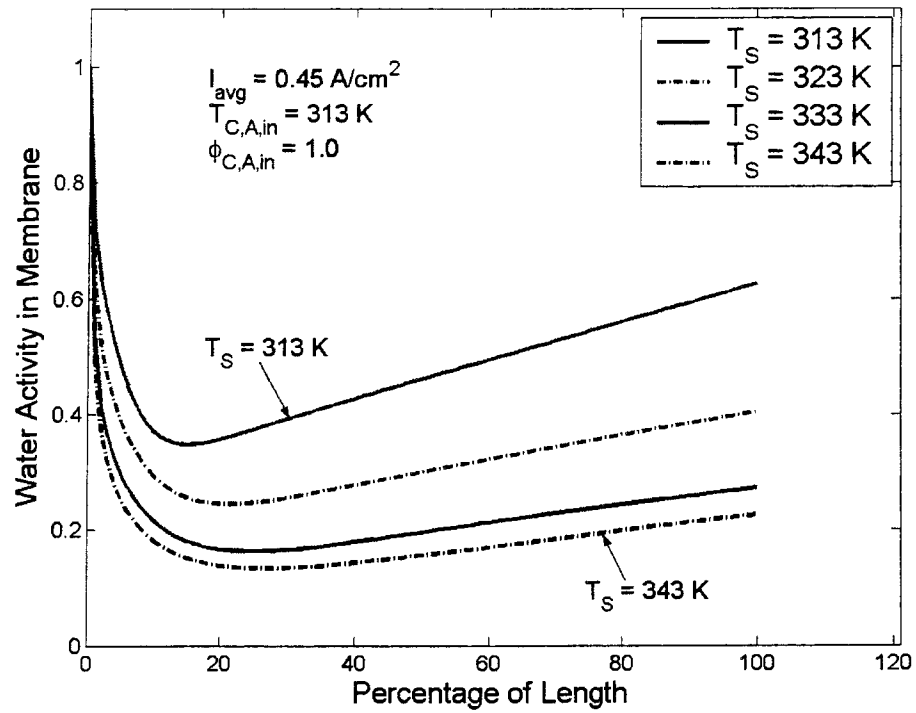
Fig. 33 A comparison of water activity in membrane along the channels with the different inlet stream temperatures.
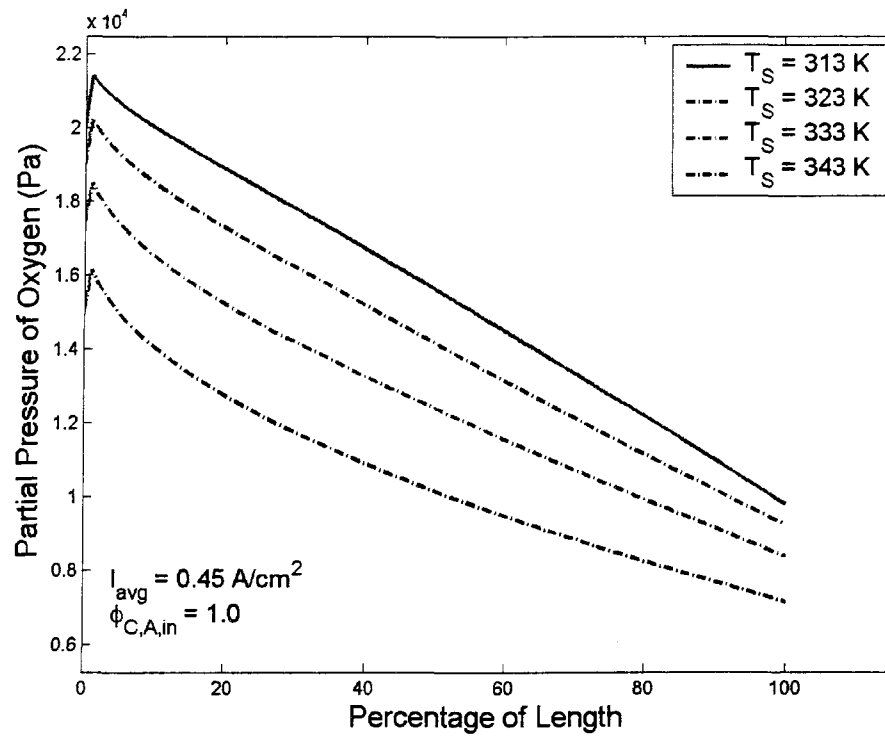
Fig. 34 A comparison of oxygen partial pressure along the channels with the different inlet flow temperatures.

Parameters	Values
Channel length (L)	83.5 cm
Channel width at cathode and anode (h)	0.15 cm
Channel height at cathode and anode (d)	0.08 cm
Channel number of cathode and anode (N_{ch})	6
The effective area	110.62 cm^2
Condensation rate constant (k_c)	1.0 s^{-1}
Membrane dry density ($\rho_{m,dry}$)	2.0 g/cm^3
Membrane dry equivalent weight ($M_{m,dry}$)	1100 g/mol
Membrane thickness (t_m)	0.01275 cm
Fuel cell open-circuit voltage (V_{oc})	1.1 V
Oxygen exchange current density (I°)	0.01 A/cm^2
Diffusion coefficient of water in membrane (D°)	5.5×10^{-7} cm^2/s

Table 1   Geometry parameters of a single fuel cell.

97

Parameters	Values
Inlet temperature of air	313 K
Inlet temperature of hydrogen	313 K
Inlet relative humidity of air	1.0
Inlet relative humidity of hydrogen	1.0
Outlet pressure of cathode	109535 Pa
Outlet pressure of anode	109535 Pa
Current density	0.5 A/cm^2
Excess coefficient of flow at cathode	2.02
Excess coefficient of flow at anode	1.169

Table 2 Operating condition in base case

VITA AUCTORIS

Yi Zong was born in 1970 in Liaoning, China. After completing high school at Fushun

No.10 High School in 1988, she went to Northeastern University and obtained her

Bachelor of Engineering in 1992. She registered in the Mechanical Engineering

Master's program at University of Windsor in 2003. Currently she is a candidate for

the Degree of Master of Applied Science in Mechanical Engineering at the University

of Windsor, Ontario, Canada.